Distributed Finite-Time Event-Triggered Frequency and Voltage Control of AC Microgrids

Jeewon Choi, Student Member, IEEE, Seyed Iman Habibi, and Ali Bidram, Senior Member, IEEE

Abstract—This paper proposes a finite-time event-triggered secondary frequency and voltage control for islanded AC microgrids (MGs) in a distributed fashion. The proposed control strategy can effectively perform frequency restoration and voltage regulations, while sharing the active and reactive power among the distributed generators (DGs) based on their power ratings. The finite-time control enables a system to reach consensus in a finite period of time enhanced from the asymptotic convergence. The event-triggered communication is utilized to reduce the communication burden among the DG controllers by transmitting data among DGs if an event-triggering condition is satisfied. The performance of the proposed finite-time event-triggered frequency control is verified utilizing a hardware-in-the-loop experimental testbed which simulates an AC MG in Opal-RT.

Index Terms—Distributed control, event-triggered control, finite-time control, islanded AC microgrid, multi-agent systems, primary control, secondary control.

I. Introduction

ICROGRIDS (MGs) as critical components of modern power systems play a significant role in increasing the reliability and resilience while facilitating the integration of sustainable energy resources. The operation of MGs in both grid-tied and islanded modes is the key factor to enhance the power grid resilience during extreme events like natural disasters. As a critical component to obtain reliable and stable operations in both modes, the hierarchically structured MG control system has been surveyed in the literature [1], [2]. The hierarchical control system is composed of the primary, secondary, and tertiary control layers [1], [2]. The primary control is locally deployed by the distributed generators (DGs) to stabilize the system frequency/voltage and to satisfy the power sharing among DGs after the MG is disconnected from the upstream power network. The secondary control restores the frequency/voltage deviations caused by the primary control. The tertiary control regulates the power flow between the main grid and the MG in grid-tied mode [1]. Traditionally, a centralized controller collects information from every DG in the secondary control layer, containing risk of being a single point of failure. As opposed to the centralized control, the distributed controllers need to interchange information only with their neighboring controllers. Such distributed secondary control architecture can increase the MG system reliability and scalability, as well as improving the computational efficiency [3]-

USA (e-mail: habibi@unm.edu; bidram@unm.edu).

[6]. The decentralized secondary control of AC microgrids has been proposed in [7]. Even though the decentralized secondary control obviates the requirement for a communication network, it still relies on the primary control level and it is not effective for some secondary control applications like regulating the voltage of a critical remote bus.

The distributed secondary control scheme has been further advanced by adopting the various control techniques. The finite-time control strategy enables a system to converge to the steady state in a finite amount of time, enhanced from the asymptotic convergence time [8]–[10]. With finite-time control, the microgrid's voltage and frequency will be converged faster to their nominal values and experience much less transients. Both of these features are very important for the microgrid critical loads. According to [11], voltage and frequency transients can result in machinery malfunction as well as microgrid's equipment and components damage and failure over time. The frameworks for the frequency/voltage restoration and active/reactive power sharing of an islanded AC MG using the finite-time control method have been introduced in the literature [12]-[14]. The frameworks introduced in [12]–[15] validates the effectiveness of finite-time secondary control in MG system, as well as presenting its robustness against the disturbances such as load changes.

Even though the distributed finite-time control techniques improve the frequency restoration speed of MGs, the DG local controllers continuously transfer their local information to other DGs which incurs unnecessary burden on the communication system. Recently, the event-triggered communication has been applied to the multi-agent systems (MAS) [16]-[18] to tackle this challenge. As apposed to the periodic communication between the agents in a conventional MAS, the eventtriggered method activates the communication only if an eventtriggering condition is satisfied, which in turn leads to the communication burden reduction. The event-triggered control has been applied to the conventional MG distributed control systems in order to decrease the communication network traffic among DGs in [19]–[26]. The complete framework for the secondary frequency/voltage restoration and active/reactive power sharing of AC MGs using the event-triggered communication is presented by [20]. The effectiveness of the eventtriggered control in the distributed secondary control under the various scenarios, such as a network delay, noise in the eventtriggering, load changes, and plug and play functionality of DG, is evaluated in [19], [21]–[23].

The aforementioned event-triggered strategies can only provide the asymptotic consensus of MAS. In practical situations however, it is desired to obtain the finite-time consensus. On

J. Choi is with the Department of Mechanical Engineering, University of New Mexico, Albuquerque, NM, 87131 USA (e-mail: chatchi923@unm.edu). S. I. Habibi and A. Bidram are with the Department of Electrical and Computer Engineering, University of New Mexico, Albuquerque, NM, 87131

that account, numerous tactics to attain a finite-time consensus under the event-triggered communication in a general MAS are introduced in the literature [27]-[34]; however, the eventtriggering mechanisms designed in [27]-[33] either require a continuous transmit of information from the neighbors or cannot guarantee the exclusion of Zeno behavior. In order to pursue a finite-time consensus with an event-triggering communication that excludess a Zeno behavior, Du et al. proposed a finite-time event-triggered consensus (FETC) scheme in [34].

Although FETC has been proposed in the literature for a general MAS, the FETC of the MG distributed control system has not been addressed in the literature. The existing distributed secondary control techniques either address the event-triggered operation or the finite-time consensus. A comprehensive distributed secondary control approach that accommodates a finite-time control response while obviating the requirements for a continuous communication is missing in the literature. Therefore, this paper creates a unified distributed secondary control for MGs that accommodates both the eventtriggered communication and finite-time response features. To this end, this paper makes the following contributions:

- 1) A FETC scheme for the MG's distributed secondary frequency and voltage control is created to achieve both consensus in finite time and lower communication burden in the MG communication system.
- 2) The exclusion of Zeno behavior in the proposed distributed frequency and voltage control is investigated.
- 3) A strategy is proposed to effectively accommodate an islanded MG's frequency and voltage control subsequent to load changes as well as energization or outage of DGs.

The remaining of this paper includes the following sections: In Section II, the primary and the secondary control levels are introduced. The distributed secondary frequency and voltage restoration framework based on the event-triggered finitetime control is proposed in Section III. The validation of the proposed secondary control through a hardware-in-theloop (HIL) simulation is presented in Section IV. Section V concludes the paper.

II. INVERTER-BASED MGS

This paper assumes that the AC MG is composed of inverter-based DGs. The block diagram of an inverter-based DG is depicted in Fig. 1. An inverter-based DG consists of the primary DC power source, inverter bridge, and nested voltage, current, and power controllers. DGs are able to control the MG frequency and voltage through the local frequency and voltage droop controllers, that is the primary control layer. In Fig. 1, the droop controllers are implemented in the power controller block. The roles of the primary control layer are to stabilize the system frequency/voltage subsequent to an islanding event as well as to share the active/reactive power among the DGs based on their power ratings [2]. The primary control, however, results in the frequency/voltage drop from the nominal operating values. The secondary control is implemented in order to restore the MG's frequency/voltage to their nominal values. In this paper, the secondary frequency/voltage restorations and the active/reactive power sharings among the

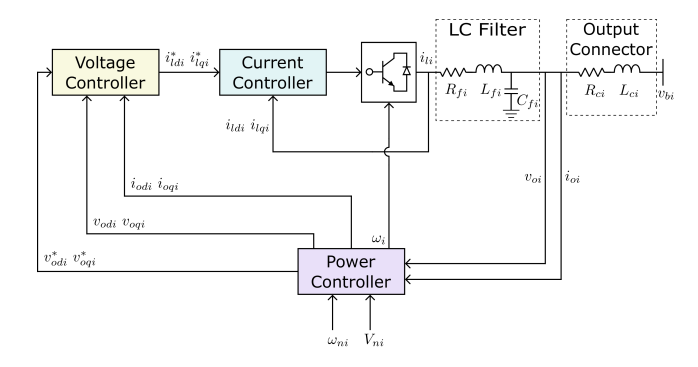


Fig. 1. Block diagram of $i^{\rm th}$ inverter-based DG.

grid-forming inverters are of concern.

The primary control is locally implemented in each inverter's controller [2]. The angular frequency ω_i and the reference value for the internal voltage controller $v_{o,\mathrm{mag}i}^*$ of DG i, are determined by the following droop characteristics

$$\omega_i = \omega_{ni} - m_{Pi} P_i \tag{1}$$

$$v_{o,\text{mag}i}^* = v_{ni} - n_{Qi}Q_i \tag{2}$$

where m_{Pi} and n_{Qi} are the active and reactive power droop coefficients, respectively, that relate to the power ratings of a DG. ω_{ni} and v_{ni} are the references for primary control. The DG's internal voltage and current controllers converge the DG's terminal voltage magnitude $v_{o,\text{mag}i}$ to $v_{o,\text{mag}i}^*$. The active/reactive power are distributed among the DGs by the primary controller proportional to their active/reactive power ratings, $P_{\max,i}$ and $Q_{\max,i}$, respectively. To this end, the active/reactive power ratios of each DG are defined as $P_i/P_{\max,i}$ and $Q_i/Q_{\max,i}$, respectively. The primary control ensures that the active/reactive power ratios satisfy

$$\frac{P_1}{P_{\text{max},1}} = \dots = \frac{P_N}{P_{\text{max},N}}$$

$$\frac{Q_1}{Q_{\text{max},1}} = \dots = \frac{Q_N}{Q_{\text{max},N}}.$$
(3)

$$\frac{Q_1}{Q_{\text{max},1}} = \dots = \frac{Q_N}{Q_{\text{max},N}}.$$
 (4)

Since the droop coefficients are selected based on the power ratings, (3)-(4) can be equivalently expressed as

$$m_{P1}P_1 = \dots = m_{PN}P_N \tag{5}$$

$$n_{Q1}Q_1 = \dots = n_{QN}Q_N. \tag{6}$$

It should be noted that once the DGs' active/reactive powers satisfy (5)-(6), the angular frequencies ω_i and voltage magnitudes $v_{o,magi}$, are settled into the values that are smaller than the nominal values. To restore MG's frequency and voltage back to the nominal values, the secondary frequency and voltage controls adjust ω_{ni} and v_{ni} of each DG in (1) and (2), respectively. This process will be discussed in Section III.

III. FETC-BASED SECONDARY FREQUENCY CONTROL

One of the objectives of an islanded MG control in the secondary level is to synchronize the angular frequencies of DGs, ω_i 's, to the nominal angular frequency of the system, $\omega_{\mathrm{ref}}.$ At the same time, it needs to allocate DGs' active powers based on their ratings according to (5). The schematic of the FETC-based secondary frequency control proposed is illustrated in Fig. 2. The secondary controller calculates the primary control input using its local and neighbors' information. The secondary controllers share information via communication graph, when the event-triggering condition is satisfied. The details of the secondary frequency controller using the FETC strategy are elaborated as follows.

A. FETC Problem for a General Linear MAS

Using input-output feedback linearization, the nonlinear dynamics of DGs are transformed to identical linear dynamics. This process has been explained in details in [35]. Based on the dependence of DGs' operating frequency and terminal voltage magnitude on the active and reactive power droop reference values, feedback linearization leads to a first-order linear tracking synchronization problem for a MAS [4]. Consider a MAS of which i^{th} agent's dynamics is given by

$$\dot{x}_i(t) = Ax_i(t) + Bu_i(t). \tag{7}$$

where $x_i(t) \in \mathbb{R}^n$ is the state variable vector, $u_i(t) \in \mathbb{R}^m$ is the system input vector, $A \in \mathbb{R}^{n \times n}$ is the state matrix and $B \in \mathbb{R}^{n \times m}$ is the input matrix. DGs can communicate with each other through a communication network which can be modeled by a graph $\mathcal{G} = (\mathcal{V}, \mathcal{E})$, where $\mathcal{V} = \{v_1, \dots, v_N\}$ is a set of N vertices or nodes, and $\mathcal{E} \subset \mathcal{V} \times \mathcal{V}$ is a set of links. The weights a_{ij} of the edges (v_i, v_i) form an adjacency matrix $\mathcal{A} = [a_{ij}] \in \mathbb{R}^{N \times N}$ of graph \mathcal{G} . If $(v_j, v_i) \in \mathcal{E}$, then $a_{ij} > 0$, otherwise $a_{ij} = 0$. The neighbors of node i are defined by a set of nodes that have a link to v_i and can be written as $\mathcal{N}_i = \{v_j | (v_j, v_i) \in \mathcal{E}\}$. The in-degree matrix of a graph is defined by $\mathcal{D} = \operatorname{diag}\{d_i\} \in \mathbb{R}^{N \times N}$ where $d_i = \sum_{j=1}^{N} a_{ij}$. The graph Laplacian matrix is calculated by $\mathcal{L} = \mathcal{D} - \mathcal{A}$ [36].

In [34], the following control input is proposed in order to achieve the finite-time consensus without continuous communication among agents

$$u_i(t) = c_1 K z_i(t) + c_2 K \operatorname{sig}(R(z_i(t) + e_i(t)))^p$$
 (8)

where $sig(x)^p = sgn(x)|x|^p$ with $0 , and <math>sgn(\cdot)$ is the signum function. c_1 and c_2 are positive real numbers, $R \in \mathbb{R}^{n \times n}$ is a positive-definite matrix, and $K = -B^{\top}R \in$ $\mathbb{R}^{m \times n}$. The estimate error $e_i(t)$ and the local tracking error $z_i(t)$ for i^{th} agent are defined as

$$e_i(t) = x_i(t) - e^{A(t - t_k^i)} x_i(t_k^i)$$
 (9)

$$z_i(t) = \sum_{j \in \mathcal{N}_i} a_{ij} \left(e^{A(t - t_k^i)} x_i(t_k^i) - e^{A(t - t_k^j)} x_j(t_k^j) \right)$$
 (10)

where t_k^i is the latest communication triggered time of $i^{ ext{th}}$ agent determined when the event-triggering condition $f_i(t) \ge$ 0 is met. To obtain the finite-time consensus, the following event-triggering function is proposed in [34]

$$f_{i}(t, e_{i}(t), z_{i}(t), \varphi_{i}(t)) = \alpha \|e_{i}(t)\|^{2} + \beta \|e_{i}(t)\|^{2p} + \gamma \|z_{i}(t)\|^{2p} - \chi \varepsilon_{1i} |\varphi_{i}(t)|^{2\psi}$$
(11)

$$\dot{\varphi}_i(t) = -\varepsilon_{2i} \operatorname{sig}(\varphi_i(t))^{\psi} \tag{12}$$

where $\alpha \|e_i(t)\|^2 + \beta \|e_i(t)\|^{2p} + \gamma \|z_i(t)\|^{2p}$ is the error term and $\chi \varepsilon_{1i} |\varphi_i(t)|^{2\psi}$ is the event-triggering threshold. The triggering condition $f_i(t) \ge 0$ indicates that the communication is triggered when the error term exceeds the threshold, i.e., agent i broadcasts its updated state $x_i(t_k^i)$ to its neighbors. Unlike the asymptotic triggering thresholds introduced in the literature [16]–[23], [26], note that the threshold $\varphi_i(t)$ developed by (12) is a positive real number that monotonically decreases to zero in finite time [34]. The term $\|e_i(t)\|^{2p}$ also helps obtaining the finite-time consensus [34]. α , β , and γ are positive real numbers greater than certain criteria, $\varepsilon_{2i} > \varepsilon_{1i} > 0$, $\chi > 0$, and $0 < \psi \le p$. The FETC strategy introduced can be summarized as Lemma 1.

Lemma 1 [34]: For the MAS given in (7), assume (A, B)is controllable and the communication graph \mathcal{G} is strongly connected. With the control law (8) and the event-triggering function (11), the system can reach consensus in finite-time for all initial conditions if the following condition is satisfied: $(\frac{c_1}{\theta_1} + \frac{c_2}{\theta_2})\lambda_{\max}(RBB^{\top}R) + \epsilon \frac{\theta_3}{2} < -\lambda_{\max}(\Xi \otimes S)$ where $\theta_1, \theta_2, \epsilon, \theta_3 > 0$.

The detailed definitions of the parameters are given in the following sequence. Note that $\lambda_i(\cdot)$ denotes the i^{th} largest eigenvalue of (\cdot) .

- 1) Solve $XA^{\top} + AX 2BB^{\top} < 0$ to get a solution X > 0. Then, $R = X^{-1}$.
- 2) Select $c_1 > \frac{1}{a(\mathcal{L})}$ that satisfies $S = RA + A^{\top}R$ $2c_1a(\mathcal{L})RBB^{\top}R < 0$ while leading to the best asymptotic consensus. The general algebraic connectivity $a(\mathcal{L})$ can be found in Definition 2. Select $c_2 > 0$ that satisfies $\tilde{S} = RA + A^{T}R - c_{2}RBB^{T}R < 0$, and 0that performs a desired finite-time consensus.
- Select $\theta_1, \theta_2, \epsilon, \theta_3 > 0$ that satisfies $(\frac{c_1}{\theta_1} + \frac{c_2}{\theta_2})\lambda_{\max}(RBB^\top R) + \epsilon \frac{\theta_3}{2} < -\lambda_{\max}(\Xi \otimes S)$ with Ξ defined in Lemma 2.
- 4) Select

 - $\alpha > c_{1}\theta_{1}\lambda_{\max}(\mathcal{L}^{\top}\Xi^{2}\mathcal{L} \otimes RBB^{\top}R) + \epsilon \frac{\|I_{N}\otimes RA \mathcal{L}\otimes R(A+c_{1}BK)\|^{2}}{2\theta_{4}}$ $\beta > \bar{c}2^{p}(Nn)^{1-p}(\|(\mathcal{L}-I_{N})\otimes R\|^{2p} + 2^{p}\|\mathcal{L}\otimes R\|^{2p}) \rho\epsilon\lambda_{\max}(\tilde{S})\|(\mathcal{L}-I_{N})\otimes R\|^{2p}$ $\gamma > 2^{2p}\bar{c}(Nn)^{1-p}\|R\|^{2p}$

 - $\bullet \stackrel{\cdot}{c} = \stackrel{\cdot}{c_2\theta_2} \lambda_{\max} \stackrel{\cdot}{(M^\top \Xi^2 M} \otimes RBB^\top R) + \epsilon \frac{\lambda_{\max}(\mathcal{L}\mathcal{L}^\top \otimes R(A+c_1BK)(A+c_1BK)^\top R)}{2\theta_3} + \epsilon \frac{\theta_4}{2} + \epsilon \|A^\top R + RA\| > 0$

where $\theta_4 > 0$, $\epsilon > 0$, $0 < \rho < 1$, and $M = I_N - \mathbf{1}_N \xi$. Note that Ξ and ξ are defined in Lemma 2.

Lemma 2 [37]: Consider a strongly connected graph \mathcal{G} with Laplacian matrix \mathcal{L} . The general algebraic connectivity of \mathcal{G} is defined by $a(\mathcal{L}) = \min_{x^{\top}\xi, x \neq 0} \frac{x^{\top}\hat{\mathcal{L}}x}{x^{\top}\Xi x}$ where $\hat{\mathcal{L}} = (\Xi\mathcal{L} + \mathcal{L}^{\top}\Xi)/2$, $\Xi = \mathrm{diag}(\xi_1, \xi_2, \cdots, \xi_N)$, $\xi = [\xi_1, \xi_2, \cdots, \xi_N]^{\top}$, $\xi^{\top}\mathcal{L} = 0$, and $\sum_{i=1}^N \xi_i = 1$. Note that the general algebraic connectivity of an undirected graph is $a(\mathcal{L}) = \lambda_2(\mathcal{L})$.

Lemma 3 [34]: If the graph is strongly connected, and the system (A, B) is controllable, there exist matrices $U \in$ $\mathbb{C}^{N\times N},\ W\in\mathbb{C}^{(N-1)\times N},\ \text{and}\ Y\in\mathbb{C}^{N\times (N-1)}\ \text{such that}$ $U^{-1}\mathcal{L}U=J_{\mathcal{L}}=\begin{bmatrix}0&\mathbf{0}_{N-1}^{\top}\\\mathbf{0}_{N-1}&\Delta\end{bmatrix},\ U^{-1}=\begin{bmatrix}\xi^{\top}\\W\end{bmatrix},\ \text{and}\ \ U=$

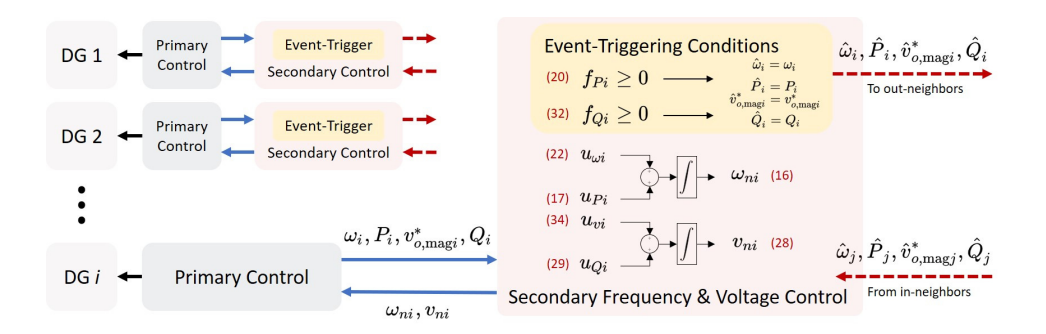


Fig. 2. Schematic of the proposed distributed FETC secondary frequency and voltage control.

 $egin{bmatrix} \mathbf{1}_N & Y \end{bmatrix}$, where $J_{\mathcal{L}}$ is the Jordan canonical form of \mathcal{L} and $\Delta \in \mathbb{C}^{(N-1) imes (N-1)}$ is a diagonal matrix.

Lemma 4 [38]: Consider a continuous nonlinear system $\dot{x} = f(x)$ with f(0) = 0. Suppose there exists a continuously differentiable function V(x) and real numbers a > 0, 0 < b < 1 that satisfy the following conditions: 1) V(x) is positive-definite; 2) $\dot{V}(x) \leq -a(V(x))^b$. Then, the settling time can be upper bounded as follows: $T(x_0) \leq \frac{1}{a(1-b)}V(x_0)^{1-b}$.

B. FETC Problem for a Secondary Frequency Control of MG
Differentiating the droop characteristic in (1) yields

$$\dot{\omega}_{ni}(t) = \dot{\omega}_i(t) + m_{Pi}\dot{P}_i(t). \tag{13}$$

Define the auxiliary frequency and active power control inputs $u_{\omega i}$ and u_{Pi} , respectively, as

$$\dot{\omega}_i(t) = u_{\omega i}(t) \tag{14}$$

$$m_{Pi}\dot{P}_i(t) = u_{Pi}(t). \tag{15}$$

From (13), the control input ω_{ni} can be written as

$$\omega_{ni} = \int (u_{\omega i} + u_{Pi})dt. \tag{16}$$

Remark 1: Note that (14)-(15) and (26)-(27) are the subcases of (7) where $A=0,\ B=1,$ and n=1.

Remark 2: Considering Remark 1, the system already satisfies $XA^{\top} + AX - 2BB^{\top} < 0$. An arbitrary solution of X=1 that is X>0 is chosen, and in turn, a positive-definite matrix of $R=X^{-1}=1$ can be determined. Then, $K=-B^{\top}R=-1$ can be decided accordingly.

1) Active Power Sharing: Utilizing (8) and considering Remark 2, the auxiliary active power control input in (15) is defined as

$$u_{Pi}(t) = -c_{P1}z_{Pi}(t) - c_{P2}\operatorname{sig}(z_{Pi}(t) + e_{Pi}(t))^{p_P}.$$
 (17)

The estimate error $e_{Pi}(t)$ and the local regulating error $z_{Pi}(t)$ for the active power sharing are defined as

$$e_{Pi}(t) = m_{Pi}P_i(t) - m_{Pi}\hat{P}_i(t)$$
 (18)

$$z_{Pi}(t) = \sum_{j \in \mathcal{N}_i} a_{ij} (m_{Pi} \hat{P}_i(t) - m_{Pj} \hat{P}_j(t))$$
 (19)

where $\hat{P}_i(t) = P_i(t_k^i)$, $t \in [t_k^i, t_{k+1}^i)$. The event-triggering time t_k^i for agent i is generated when the event-triggering

condition $f_{Pi}(t) \ge 0$ is satisfied. The event-triggering function $f_{Pi}(t)$ is defined by

$$f_{Pi}(t, e_{Pi}, z_{Pi}, \varphi_{Pi}) = \alpha_P \|e_{Pi}\|^2 + \beta_P \|e_{Pi}\|^{2p_P} + \gamma_P \|z_{Pi}\|^{2p_P} - \chi_P \varepsilon_{P1i} |\varphi_{Pi}|^{2\psi_P}$$
(20)

$$\dot{\varphi}_{Pi}(t) = -\varepsilon_{P2i} \operatorname{sig}(\varphi_{Pi}(t))^{\psi_P}. \tag{21}$$

The finite-time convergence of the active power sharing using (17) and (20) is achieved according to Lemma 1.

2) Frequency Restoration: Similar to the active power sharing, the auxiliary frequency control input (14) is formulated as

$$u_{\omega i}(t) = -c_{\omega 1} z_{\omega i}(t) - c_{\omega 2} \operatorname{sig}(z_{\omega i}(t) + e_{\omega i}(t))^{p_{\omega}}. \tag{22}$$

The estimate error $e_{\omega i}(t)$ and the local tracking error $z_{\omega i}(t)$ for frequency control are respectively defined as

$$e_{\omega i}(t) = \omega_i(t) - \hat{\omega}_i(t) \tag{23}$$

$$z_{\omega i}(t) = \sum_{j \in \mathcal{N}_i} a_{ij} (\hat{\omega_i}(t) - \hat{\omega}_j(t)) + g_i (\hat{\omega}_i(t) - \omega_{\text{ref}}) \quad (24)$$

where $\hat{\omega}_i(t) = \omega_i(t_k^i)$, $t \in [t_k^i, t_{k+1}^i)$. Note from (24) that the frequency control is a leader-follower problem. In the leader-follower problem, the pinning gain g_i is greater than zero only if the corresponding i^{th} DG has a direct edge to the leader node, i.e., DG i receives the reference value ω_{ref} . g_i equals to zero otherwise. According to Remark 3, the event-triggering time for agent i is also determined when $f_{Pi}(t) \geq 0$. According to Lemma 1, using (20) and (22), the frequency synchronization can be reached in finite time for any initial conditions as long as the condition in Lemma 1 is satisfied.

Remark 3: The frequency and voltage control has faster dynamics than the power sharing controls, that is, the stabilization time holds $T_c^P \approx 10 T_c^\omega$ and $T_c^Q \approx 10 T_c^v$; therefore the frequency/voltage reaches the steady state faster than the active/reactive power. Generally, the controllers share one common communication network, therefore using two separate triggering conditions in a different timescale is likely to incur excessive communication [26].

C. FETC Problem for a Secondary Voltage Control of MG

Similar to the frequency control, differentiate the reactive power droop characteristic (2) to obtain the following:

$$\dot{v}_{ni}(t) = \dot{v}_{o,\text{mag}i}^{*}(t) + n_{Qi}\dot{Q}_{i}(t).$$
 (25)

Define the auxiliary voltage and reactive power control inputs, u_{vi} and u_{Qi} , as follows:

$$\dot{v}_{o,\text{mag}i}^*(t) = u_{vi}(t) \tag{26}$$

$$n_{Qi}\dot{Q}_i(t) = u_{Qi}(t). \tag{27}$$

By combining (25)-(27), the secondary voltage control input v_{ni} can be defined as

$$v_{ni} = \int (u_{vi} + u_{Qi})dt. \tag{28}$$

1) Reactive Power Sharing: Utilizing (8) and considering Remark 2, the auxiliary reactive power control input u_{Qi} can be written as

$$u_{Qi}(t) = -c_{Q1}z_{Qi}(t) - c_{Q2}\operatorname{sig}(z_{Qi}(t) + e_{Qi}(t))^{p_Q}.$$
 (29)

The estimate error $e_{Qi(t)}$ and the local tracking error $z_{Qi}(t)$ for the reactive power sharing can be defined as

$$e_{Qi}(t) = n_{Qi}Q_i(t) - n_{Qi}\hat{Q}_i(t)$$
 (30)

$$z_{Qi}(t) = \sum_{j \in \mathcal{N}_i} a_{ij} (n_{Qi} \hat{Q}_i(t) - n_{Qj} \hat{Q}_j(t)).$$
 (31)

Considering Remark 3, the reactive power and voltage measurements can be updated using the event-triggering condition in terms of reactive powers. Utilizing (8) and (12), the event-triggering condition $f_{Oi}(t)$ can be formulated as

$$f_{Qi}(t, e_{Qi}, z_{Qi}, \varphi_{Qi}) = \alpha_Q \|e_{Qi}\|^2 + \beta_Q \|e_{Qi}\|^{2p_Q} + \gamma_Q \|z_{Qi}\|^{2p_Q} - \chi_Q \varepsilon_{Q1i} |\varphi_{Qi}|^{2\psi_Q}$$
(32)

$$\dot{\varphi}_{Oi}(t) = -\varepsilon_{O2i} \operatorname{sig}(\varphi_{Oi}(t))^{\psi_Q}. \tag{33}$$

2) Voltage Restoration: Equivalent to the frequency control, the auxiliary voltage control input can be written as

$$u_{vi}(t) = -c_{v1}z_{vi}(t) - c_{v2}\operatorname{sig}(z_{vi}(t) + e_{vi}(t))^{p_v}.$$
 (34)

The estimate error $e_{vi}(t)$ and the local tracking error $z_{vi}(t)$ for the voltage control are defined as

$$e_{vi}(t) = v_{o,\text{mag}i}(t) - \hat{v}_{o,\text{mag}i}(t)$$
(35)

$$z_{vi}(t) = \sum_{j \in \mathcal{N}_i} a_{ij}(\hat{v}_{o,\text{mag}i}(t) - \hat{v}_{o,\text{mag}j}(t)) +g_i(\hat{v}_{o,\text{mag}i}(t) - v_{\text{ref}}).$$
(36)

If the voltage of a critical bus of microgrid is desired to be synchronized to the nominal voltage, the reference voltage in the auxiliary voltage input can be chosen as

$$v_{\text{ref}} = k_p(v_{\text{nom}} - v_{\text{crit}}) + k_i(v_{\text{nom}} - v_{\text{crit}})$$
 (37)

where $v_{\rm crit}$ is the critical bus voltage, k_i and k_p are PI control gains. According to Lemma 1 and Remark 3, the reactive power sharing and the voltage restoration can be achieved in finite amount of time using (32) and (33).

D. Finite-Time Stability

The secondary control problem of an islanded AC MG consists of four MAS regulation/tracking problems, namely frequency restoration, active power sharing, voltage restoration, and reactive power sharing. Since these problems are similarly structured, herein, the finite-time stability of active power sharing problem is discussed on behalf of secondary control problems without loss of generality. Denote $m_{Pi}P_i(t) = P_{mi}(t)$ for simplicity. The active power sharing problem can be expressed as the following matrix form by combining (15), (17)-(19):

$$\dot{P}_m(t) = -c_{P1}\mathcal{L}(P_m(t) - e_P(t)) -c_{P2}\operatorname{sig}(\mathcal{L}(P_m(t) - e_P(t)) + e_P(t))^{p_P}$$
(38)

where $P_m(t) = [P_{m1}(t), \cdots, P_{mN}(t)]^{\top}$ and $e_P(t) = [e_{P1}(t), \cdots, e_{PN}(t)]^{\top}$. Define a disagreement vector $\vartheta_P(t) = (I_N - \mathbf{1}_N \xi^{\top}) P_m(t)$, then its derivative can be written as

$$\dot{\vartheta}_P(t) = -c_{P1}\mathcal{L}(\vartheta(t) - e_P(t)) -c_{P2}M\operatorname{sig}(\mathcal{L}(\vartheta(t) - e_P(t)) + I_N e_P(t))^{p_P}$$
(39)

where $M = I_N - \mathbf{1}_N \xi^{\mathsf{T}}$. Note that $M\mathcal{L} = \mathcal{L}$ since $\xi^{\mathsf{T}} \mathcal{L} = 0$. Then, finite-time convergence of the active power sharing problem in terms of the disagreement vector is investigated over microscopic and macroscopic time periods, i.e., convergence between two events where there is no event triggered in between, and convergence over the entire time period [34].

Finite-time convergence between events [34]: First, Lyapunov stability during the communication intervals is discussed. For further simplicity, the time term t and subscript P are omitted. Select the following Lyapunov function candidate

$$V = V_1 + V_2 + V_3 (40)$$

$$V_1 = \vartheta^\top \Xi \vartheta \tag{41}$$

$$V_2 = \sum_{i=1}^{N} \frac{\epsilon}{1+p} |q_i|^{p+1} \tag{42}$$

$$V_3 = \sum_{i=1}^{N} \frac{\chi}{1+\psi} |\varphi_i|^{1+\psi}$$
 (43)

where $q = \mathcal{L}(\vartheta - e) + e = [q_1, \dots, q_N]^{\top}$ [34]. The derivative of V_1 and its upper bound is found as

$$\dot{V}_{1} = \dot{\vartheta}^{\top} \Xi \vartheta + \vartheta \Xi \dot{\vartheta}
= -2c_{1}\vartheta^{\top} \Xi \mathcal{L}\vartheta + 2c_{1}\vartheta^{\top} \Xi \mathcal{L}e - 2c_{2}\vartheta^{\top} \Xi M \operatorname{sig}(q)^{p}
\leq \lambda_{\max}(\Xi \otimes S) \|\vartheta\|^{2}
+ \frac{c_{1}}{\theta_{1}} \|\vartheta\|^{2} + c_{1}\theta_{1}\lambda_{\max}(\mathcal{L}^{\top} \Xi^{2} \mathcal{L}) \|e\|^{2}
+ \frac{c_{2}}{\theta_{2}} \|\vartheta\|^{2} + c_{2}\theta_{2}\lambda_{\max}(M^{\top} \Xi^{2} M)
\times (\operatorname{sig}(q)^{p})^{\top} \operatorname{sig}(q)^{p}$$
(44)

where θ_1 and θ_2 are Young's inequality parameters used to bound \dot{V}_1 . Note that Young's inequality parameters can be

any positive numbers that satisfy the condition in Lemma 1. The derivative of V_2 can be found and bounded as

$$\dot{V}_{2} = \epsilon \sum_{i=1}^{N} \operatorname{sig}(q_{i})^{p} \dot{q}_{i}$$

$$= \epsilon (\operatorname{sig}(q)^{p})^{\top} (-c_{1}\mathcal{L})\vartheta + \epsilon (\operatorname{sig}(q)^{p})^{\top} (c_{1}\mathcal{L})e$$

$$+ \epsilon (\operatorname{sig}(q)^{p})^{\top} (\tilde{S})\operatorname{sig}(q)^{p}$$

$$\leq \frac{\epsilon \lambda_{\max}(c_{1}^{2}\mathcal{L}^{\top}\mathcal{L})}{2\theta_{3}} (\operatorname{sig}(q)^{p})^{\top} \operatorname{sig}(q)^{p} + \frac{\epsilon \theta_{3}}{2} \|\vartheta\|^{2}$$

$$+ \frac{\epsilon \|c_{1}\mathcal{L}\|^{2}}{2\theta_{4}} \|e\|^{2} + \frac{\epsilon \theta_{4}}{2} (\operatorname{sig}(q)^{p})^{\top} \operatorname{sig}(q)^{p}$$

$$+ \epsilon \lambda_{\max}(\tilde{S}) (\operatorname{sig}(q)^{p})^{\top} \operatorname{sig}(q)^{p}$$
(45)

where θ_3 and θ_4 are Young's inequality parameters. Since φ_i is a predesignated function, the derivative of V_3 can be written as

$$\dot{V}_3 = \chi \sum_{i=1}^{N} \operatorname{sig}(\varphi_i)^{\psi} \dot{\varphi}_i = -\chi \varepsilon_{2i} \sum_{i=1}^{N} |\varphi_i|^{2\psi}. \tag{46}$$

Combining (44)-(46) yields,

$$\dot{V} \leq \left(\lambda_{\max}(\Xi \otimes S) + \frac{c_1}{\theta_1} + \frac{c_2}{\theta_2} + \frac{\epsilon \theta_3}{2}\right) \|\vartheta\|^2 \\
+ \left(c_1 \theta_1 \lambda_{\max}(\mathcal{L}^\top \Xi^2 \mathcal{L}) + \frac{\epsilon \|c_1 \mathcal{L}\|^2}{2\theta_4}\right) \|e\|^2 \\
+ \left(\bar{c} + \rho \epsilon \lambda_{\max}(\tilde{S}) + (1 - \rho)\epsilon \lambda_{\max}(\tilde{S})\right) \\
\times (\operatorname{sig}(q)^p)^\top \operatorname{sig}(q)^p - \chi \varepsilon_{2i} \sum_{i=1}^N |\varphi_i|^{2\psi}$$
(47)

where $\bar{c}=c_2\theta_2\lambda_{\max}(M^{\top}\Xi^2M)+\frac{\epsilon\lambda_{\max}(c_1^2\mathcal{LL}^{\top})}{2\theta_2}+\frac{\epsilon\theta_4}{2}$ and $0<\rho<1$ [34]. Using $\|\mathcal{L}\vartheta\|^{2p}=\|z+\mathcal{L}e\|^{2p}\leq 2^p\|z\|^{2p}+2^p\|\mathcal{L}\|^{2p}\|e\|^{2p}$, the upper bounds for the third term elements in (47) are found as follows [34]:

$$\bar{c}(\operatorname{sig}(q)^{p})^{\top} \operatorname{sig}(q)^{p} \leq \bar{c}2^{p} N^{1-p} (\|\mathcal{L}\vartheta\|^{2p} + \|\mathcal{L}e - e\|^{2p})
\leq \bar{c}2^{2p} N^{1-p} \|z\|^{2p} + \bar{c}2^{p} N^{1-p} \times$$

$$(2^{p} \|\mathcal{L}\|^{2p} + \|\mathcal{L} - I_{N}\|^{2p}) \|e\|^{2p},$$
(48)

$$\rho \epsilon \lambda_{\max}(\tilde{S})(\operatorname{sig}(q)^{p})^{\top} \operatorname{sig}(q)^{p}$$

$$\leq \rho \epsilon \lambda_{\max}(\tilde{S}) \|\mathcal{L}\vartheta\|^{2p} - \rho \epsilon \lambda_{\max}(\tilde{S}) \|\mathcal{L}e - e\|^{2p}$$

$$\leq \rho \epsilon \lambda_{\max}(\tilde{S}) \|\mathcal{L}\vartheta\|^{2p} - \rho \epsilon \lambda_{\max}(\tilde{S}) \|\mathcal{L} - I_{N}\|^{2p} \|e\|^{2p}.$$
(49)

Then, the inequality (47) can be further bounded by

$$\dot{V} \leq \left(\lambda_{\max}(\Xi \otimes S) + \frac{c_{1}}{\theta_{1}} + \frac{c_{2}}{\theta_{2}} + \frac{\epsilon\theta_{3}}{2}\right) \|\vartheta\|^{2}
+ \left(c_{1}\theta_{1}\lambda_{\max}(\mathcal{L}^{\top}\Xi^{2}\mathcal{L}) + \frac{\epsilon\|c_{1}\mathcal{L}\|^{2}}{2\theta_{4}}\right) \|e\|^{2}
+ \left(\bar{c}2^{p}N^{1-p}(2^{p}\|\mathcal{L}\|^{2p} + \|\mathcal{L} - I_{N}\|^{2p}\right)
- \rho\epsilon\lambda_{\max}(\tilde{S})\|\mathcal{L} - I_{N}\|^{2p}\right) \|e\|^{2p}
+ \left(\bar{c}2^{2p}N^{1-p}\right) \|z\|^{2p} - \chi\varepsilon_{2i}\sum_{i=1}^{N} |\varphi_{i}|^{2\psi}
+ \rho\epsilon\lambda_{\max}(\tilde{S})\|\mathcal{L}\vartheta\|^{2p}
+ (1-\rho)\epsilon\lambda_{\max}(\tilde{S})(\operatorname{sig}(q)^{p})^{\top}\operatorname{sig}(q)^{p}.$$
(50)

Assume $\lambda_{\max}(\Xi \otimes S) + \frac{c_1}{\theta_1} + \frac{c_2}{\theta_2} + \frac{\epsilon \theta_3}{2} < 0$. Replace $\|e\|^2$, $\|e\|^{2p}$, and $\|z\|^{2p}$ terms by (20). Then (50) can be further bounded by

$$\dot{V} \leq \rho \epsilon \lambda_{\max}(\tilde{S}) \|\mathcal{L}\vartheta\|^{2p}
+ (1-\rho)\epsilon \lambda_{\max}(\tilde{S}) (\operatorname{sig}(q)^{p})^{\top} \operatorname{sig}(q)^{p}
+ \chi(\varepsilon_{1i} - \varepsilon_{2i}) \sum_{i=1}^{N} |\varphi_{i}|^{2\psi}.$$
(51)

In order to further bound each term in (51), the state transformation $\zeta = U^{-1}\vartheta = [\zeta_1^\top, \zeta_2^\top]$ where $\zeta_1 \in \mathbb{C}$ and $\zeta_2 \in \mathbb{C}^{N-1}$, are employed [34]. Note that the matrices U, W, Y, and Δ can be defined from Lemma 3. Using the state transformation, the following can be found:

$$\zeta = \begin{bmatrix} \xi^{\top} \\ W \end{bmatrix} (I_N - \mathbf{1}_N \xi^{\top}) P_m
= \begin{bmatrix} \mathbf{0}_N^{\top} \\ W(I_N - \mathbf{1}_N \xi^{\top}) \end{bmatrix} P_m$$
(52)

From (52), ζ_1 is found to be zero. Using the fact that $\zeta_1 = 0$, $\vartheta^{\top}(\mathcal{L}^{\top}\mathcal{L})\vartheta \geq \lambda_{\min}(U^{\top}U)\lambda_{\min}(\Delta^{\top}\Delta)\zeta_2^{\top}\zeta_2$ and $\vartheta^{\top}\Xi\vartheta \leq \lambda_{\max}(U^{\top}\Xi U)\zeta_2^{\top}\zeta_2$, the first, second, and third term in (51) can be respectively bounded as follows [34]:

$$\rho \epsilon \lambda_{\max}(\tilde{S}) \| \mathcal{L} \vartheta \|^{2p}$$

$$\leq \rho \epsilon \lambda_{\max}(\tilde{Q}) \left(\frac{\lambda_{\min}(U^{\top}U) \lambda_{\min}(\Delta^{\top}\Delta)}{\lambda_{\max}(U^{\top}\Xi U)} \right)^{p} V_{1}^{p} \qquad (53)$$

$$= \alpha' V_{1}^{p},$$

$$(1 - \rho)\epsilon \lambda_{\max}(\tilde{S})(\operatorname{sig}(q)^{p})^{\top} \operatorname{sig}(q)^{p}$$

$$\leq (1 - \rho)\epsilon \lambda_{\max}(\tilde{Q}) \left(\frac{p+1}{\epsilon}\right)^{\frac{2p}{p+1}} V_{2}^{\frac{2p}{p+1}}$$

$$= \beta' V_{2}^{\frac{2p}{p+1}},$$
(54)

$$\chi(\varepsilon_{1i} - \varepsilon_{2i}) \sum_{i=1}^{N} |\varphi_i|^{2\psi}
\leq (\varepsilon_1 - \varepsilon_2) \frac{(1+\psi)^{\frac{2\psi}{1+\psi}}}{\chi^{\frac{\psi-1}{\psi+1}}} V_3^{\frac{2\psi}{\psi+1}}
= \gamma' V_3^{\frac{2\psi}{\psi+1}}.$$
(55)

Note that α' , β' , $\gamma' < 0$. Combining (53)-(55), the inequality (51) can be rewritten as

$$\dot{V} \le \alpha' V_1^p + \beta' V_2^{\frac{2p}{p+1}} + \gamma' V_3^{\frac{2\psi}{\psi+1}} \le 0.$$
 (56)

From the inequality $0<\psi\leq p\leq 0.5,\ p<\frac{2p}{p+1}$ and $\frac{2\psi}{\psi+1}\leq \frac{2p}{p+1}$ can be known easily. First, assume the case where $0< V\leq 1.$ Thus, $0< V_1\leq 1,\ 0< V_2\leq 1,$ and $0< V_3\leq 1$ also hold. Then, (56) can be rebounded as

$$\dot{V} \leq \alpha' V_{1}^{\frac{2p}{p+1}} + \beta' V_{2}^{\frac{2p}{p+1}} + \gamma' V_{3}^{\frac{2p}{p+1}}
< \max(\alpha', \beta', \gamma') (V_{1}^{\frac{2p}{p+1}} + \beta' V_{2}^{\frac{2p}{p+1}} + \gamma' V_{2}^{\frac{2p}{p+1}})
< \max(\alpha', \beta', \gamma') (V_{1} + V_{2} + V_{3})^{\frac{2p}{p+1}}
= \max(\alpha', \beta', \gamma') V_{2}^{\frac{2p}{p+1}}$$
(57)

Applying Lemma 4, V will reach zero in finite-time

$$t_f \le \frac{V(0)^{1 - \frac{2p}{p+1}}}{-\max(\alpha', \beta', \gamma')(1 - \frac{2p}{p+1})}.$$
 (58)

Now consider a case where V > 1. Based on (56), there exists a positive scalar r such that $\dot{V} \leq -r$. Then, V converges to 1 in finite time [34]. Once it reaches 1, it becomes the case where 0 < V < 1.

Finite-time convergence over entire time period [34]: Now, stability over the entire time period that includes the impact of event triggering will be discussed. Note that V_1 and V_3 are not affected by the communication triggered [34]. V_2 is going to have a jump in its value since e_i is reset to zero at its trigger time $t=t_k^i$. If the jump in V_2 results in the increase of V_2 , it may discourage V converging to zero. The value of V_2 can be bounded as

$$V_{2}(t_{k}^{i}) = \frac{\epsilon}{1+p} \left\| \mathcal{L}\vartheta(t_{k}^{i}) - (\mathcal{L} - I_{N})e(t_{k}^{i}) \right\|^{p+1}$$

$$\leq \alpha^{*} \left\| \mathcal{L}\vartheta(t_{k}^{i}) \right\|^{p+1} + \beta^{*} \left\| e(t_{k}^{i}) \right\|^{p+1}$$
(59)

where $\alpha^* = \frac{\epsilon 2^{\frac{p+1}{1}}}{1+p} N^{\frac{p+1}{2}}$ and $\beta^* = \alpha^* \| \mathcal{L} - I_N \|^{p+1}$ [34]. Denote $V_2(\underline{t}_k^i)$ and $V_2(\overline{t}_k^i)$ as values of V_2 before and after triggering at $t = t_k^i$, respectively. Then, the upper bounds for each case will be $\alpha^* \| \mathcal{L} \vartheta(\underline{t}_k^i) \|^{p+1} + \beta^* \| e(\underline{t}_k^i) \|^{p+1}$ and $\alpha^* \| \mathcal{L} \vartheta(\overline{t}_k^i) \|^{p+1} + \beta^* \| e(\overline{t}_k^i) \|^{p+1}$, respectively. It is obvious that the estimate error is smaller after triggering than before, therefore $0 \leq \| e(\overline{t}_k^i) \| \leq \| e(\underline{t}_k^i) \|$. Also, $\| \mathcal{L} \vartheta(\underline{t}_k^i) \|^{p+1} = \| \mathcal{L} \vartheta(\overline{t}_k^i) \|^{p+1}$ according to [34]. Therefore, it can be said that the upper bound of V_2 is smaller after triggering than before. For the case where V_2 has increased after triggering, the maximum magnitude of the increment is $\alpha^* \| \mathcal{L} \vartheta(\overline{t}_k^i) \|^{p+1} + \beta^* \| e(\overline{t}_k^i) \|^{p+1}$ and it can be bounded as

$$\alpha^* \left\| \mathcal{L} \vartheta(\bar{t}_k^i) \right\|^{p+1} + \beta^* \left\| e(\bar{t}_k^i) \right\|^{p+1} \\ \leq \alpha^* 2^{\frac{p+1}{2}} \left\| z(\bar{t}_k^i) \right\|^{p+1} + \gamma^* \left\| e(\bar{t}_k^i) \right\|^{p+1}$$
(60)

where $\gamma^* = \alpha^* 2^{\frac{p+1}{2}} \|\mathcal{L}\|^{p+1} + \beta^*$ [34]. From (60), it is observed that the positive increment of V_2 is bounded by $\|z(\bar{t}_k^i)\|^{p+1}$ and $\|e(\bar{t}_k^i)\|^{p+1}$ which are predestined to reach zero by the threshold (20) and (21). Then, V can converge to zero in finite time based on the convergence time discussed for interevent intervals [34].

Combining the analyses for two cases, it can be concluded that V can converge to zero in finite time. In other words, the active power sharing problem can reach consensus in finite time utilizing the control protocol (29) and the event-triggering condition (20)-(21).

E. Zeno Behavior Discussion

Due to the mechanism of event-triggered control, that is, the communication is triggered when an error term exceeds the triggering threshold, it is possible that the communication is unlimitedly triggered during a short period of time even if the error term is small but the threshold is even smaller. The aforementioned phenomenon is known as Zeno behavior, and is expected to be analyzed when solving an event-triggered control problem. To prove that Zeno behavior is excluded from the system, the minimum interevent interval needs to be bounded by a nonzero positive value.

The Zeno behavior of the proposed FETC strategy is investigated for two conditions, i.e., when $T_c < T_\varphi$ and when $T_c \geq T_\varphi$, where T_c denotes the time when the finite-time consensus is reached, and T_φ is the time when $\varphi_i(t)$ is converged to zero [34].

Zeno behavior when $T_c < T_{\varphi}$: For the active power sharing control in (15), the estimate error can be written as

$$e_{Pi}(\tau) = \int_{t_k^i}^t u_{Pi}(\tau)d\tau$$

$$= \int_{t_k^i}^t (-c_1 z_{Pi}(\tau) - c_2 \text{sig}(z_{Pi}(\tau) + e_{Pi}(\tau))^p d\tau.$$
(61)

Then the magnitude of estimate error can be bounded by

$$||e_{Pi}|| \le c_1 \int_{t_k^i}^t ||z_{Pi}|| d\tau + c_2 \int_{t_k^i}^t ||\operatorname{sig}(z_{Pi} + e_{Pi})^p)|| d\tau$$

$$= c_1 ||z_{Pi}|| (t - t_k^i) + c_2 ||\operatorname{sig}(z_{Pi} + e_{Pi})^p)|| (t - t_k^i)$$

$$= (c_1 ||z_{Pi}|| + c_2 ||\Phi||) (t - t_k^i)$$
(62)

where Φ is the upper bound of $\operatorname{sig}(z_{Pi}(t) + e_{Pi}(t))^p$; Φ can be bounded because z_{Pi} and e_{Pi} converge to zero at consensus [34]. Define the upper bound of $\|z_{Pi}\|$ as ϱ , then $c_1\|z_{Pi}\| + c_2\|\Phi\| \le c_1\varrho + c_2\|\Phi\|$, and let $\varsigma = c_1\varrho + c_2\|\Phi\|$. Consider (20) and (62), and let T_e' be the solution of

$$\alpha \varsigma^2 (T_e')^2 + \beta \varsigma^{2p} (T_e')^{2p} + \gamma \varrho^{2p} = \chi \varepsilon_{1i} |\varphi_i|^{2\psi} \qquad (63)$$

where $\alpha \varsigma^2$, $\beta \varsigma^{2p}$, and $\gamma \varrho^{2p}$ are less than $\chi \epsilon_{1i} |\varphi_i|^{2\psi}$ [34]. Then, when an event is triggered, the interevent time interval $T_e = t_{k+1}^i - t_k^i$ must be greater than or equal to T_e' . The solution of (63) satisfies $T_e' > 0$ if $\varphi_i \neq 0$ [34]. Then it can be obtained that $T_e \geq T_e' > 0$ when the threshold does not converge to zero [34]. The above analysis indicates that Zeno behavior is excluded while $\varphi_i(t) \neq 0$. Therefore for $T_c < T_{\varphi}$, Zeno behavior is excluded for the entire time since the consensus is achieved before $\varphi_i(t)$ goes to zero.

Zeno behavior when $T_c \geq T_{\varphi}$: For this case, Zeno behavior is excluded for $t < T_{\varphi}$ and $t > T_c$. Overall, Zeno behavior is excluded for $t \in [0, \min\{T_c, T_{\varphi}\}] \cup [T_c, \infty]$ for the FETC strategy introduced [34]. In fact, the exclusion of Zeno behavior can be achieved by setting a proper initial value and parameters for the threshold such that $T_c < T_{\varphi}$.

F. Strategy for MG's Frequency Restoration Subsequent to Disturbances

The secondary control is usually applied right after the MG islanding. In the proposed FETC scheme, once the islanding is detected, the event-triggering threshold $\chi \varepsilon_{1i} |\varphi_i(t)|^{2\psi}$ in (11) adopts it's initial value and the communication triggering occurs once the error term in (11) becomes greater than

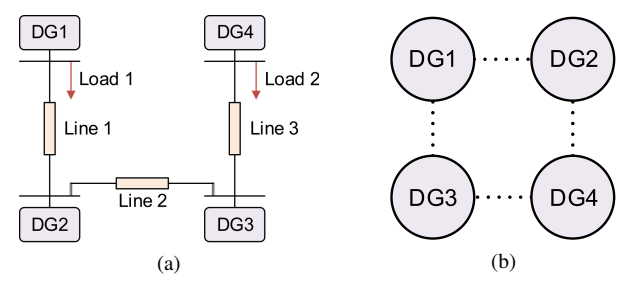


Fig. 3. 4 DG MG test system in Case A & B: (a) circuit diagram; (b) communication graph.

the threshold. In practical implementation, the triggering is inactivated when the error term remains smaller than a certain value for some amount of time, so that the secondary control can be turned off after the consensus is achieved. However, upon the occurrence of a disturbance like load change, the triggering threshold is required to reset and readopt it's initial value to accommodate a limited number of triggering events before the MG distributed frequency control restores MG's frequency to the nominal frequency. To this end, a strategy is proposed to effectively reset the triggering threshold upon the occurrence of disturbances. In the proposed strategy, the triggering threshold only resets if the error term in (11) has been less than a certain value for a specific amount of time before it crosses that value again.

IV. CASE STUDIES

In this section, the effectiveness of the proposed FETC controller is evaluated using two MG test systems. The first MG includes 4 DGs and is utilized in Cases A and B. The second MG that consists of 20 DGs is used in Case C.

A. Case A: FETC Verification for Islanded MG with 4 DGs

Case A validates the effectiveness of FETC control strategies on a $60~{\rm Hz}/480~{\rm V}$ MG test system with 4 DGs in MATLAB/Simulink environment. The single-line diagram of 4 DG MG is shown in Fig. 3a. The specifications of DGs, lines, and loads are provided in Table I. The critical bus of MG is DG 4 bus where Load 2, which is considered as a critical load, is connected.

The communication graph for Case A is illustrated in Fig. 3b where each dotted line represents a bidirectional link. The corresponding adjacency matrix to that graph is

$$\mathcal{A} = \begin{bmatrix} 0 & 1 & 1 & 0 \\ 1 & 0 & 0 & 1 \\ 1 & 0 & 0 & 1 \\ 0 & 1 & 1 & 0 \end{bmatrix}.$$

The reference frequency and voltage values $\omega_{\rm ref}$ and $v_{\rm ref}$ are sent to DG 1 from the leader node, with the pinning gain of $g_1=1$. Every DG is reachable from every other DG, therefore the graph is strongly connected. This graph is undirected and its algebraic connectivity $a(\mathcal{L})$ is 2 that is the second largest eigenvalue of \mathcal{L} . The control parameters for Case A are tabulated in Table II. φ_0 is the initial value of $\varphi(t)$.

TABLE I MG Specifications in Case A & B

DGs	DG 1, 4		DG 2, 3			
m_P	1×10^{-4}		2×10^{-4}			
n_Q	2×10^{-3}		4×10^{-3}			
$R_{\rm c}$	$0.05~\Omega$		0.05Ω			
$L_{\rm c}$	4.8 mH		4.8 mH			
$R_{ m f}$	$0.1~\Omega$		$0.1~\Omega$			
$L_{ m f}$	1.35 mH		1.35 mH			
$C_{ m f}$	$50 \mu F$		$50 \ \mu F$			
$K_{ m PV}$	0.1		0.05			
K_{IV}	420		390			
K_{PC}	15	10.5				
$K_{\rm IC}$	20000	16000				
Lines	Line 1	Line 2 Line 3				
\overline{R}	0.2 Ω	0.1 Ω	0.2 Ω			
L	3.6 mH	$1.8~\mathrm{mH}$	$3.6~\mathrm{mH}$			
Loads	Load 1	Load 2				
\overline{P}	12 kW	12 kW				
Q_L	5 kVAr	5 kVAr				

TABLE II CONTROLLER PARAMETERS IN CASE A

secondary	c_1	c_2	p	secoi	ndary	c_1	c_2	p
Frequency	10	10	0.5	Voltage		5	20	0.5
Active Power	10	10	0.5		ctive wer	5	20	0.5
Triggering Condition	α	β	γ	χ	ε_1	$arepsilon_2$	ψ	φ_0
$f_{Pi} \ f_{Qi}$	31 32	237 237	39 39	1 1	1 1	2 15	0.5 0.5	10 500

1) Case A.1. Islanding from Main Grid: The performance of the proposed secondary controller at the event of MG islanding is investigated in this test case. The response of 4 DG MG model is shown in Fig. 4 and Fig. 5. The MG is disconnected from the main grid at t = 0 s. In order to highlight the effectiveness of the proposed secondary controller, the secondary control is not applied during 0 < t < 2 s. After the disconnection, the active power ratios of DGs synchronize to an identical value satisfying (5) and the frequencies are settled around 59.89 Hz by the primary controller as shown in Fig. 4b and Fig. 4a, respectively. Even though the primary control is able to settle the DG frequencies, it cannot avoid the deviation from the nominal frequency of 60 Hz. At t = 2 s, the secondary control is activated and the frequencies are successfully restored to 60 Hz around t = 4.5 s, still achieving an accurate active power sharing. For the voltage control, $v_{\rm ref}$ is calculated from (37) with $k_p = 2$ and $k_i = 4$. Similar to the frequency control, while a proper reactive power sharing is observed as shown in Fig. 5b, the critical bus voltage is unable to settle to the nominal value without the secondary control during 0 < t < 2 s as shown in Fig. 5a. The secondary control restores the critical bus voltage to 480 V when activated, while obtaining a synchronization of reactive power ratios. Therefore, it can be said that the proposed secondary controller is capable of providing the proper active/reactive power sharings, while simultaneously fulfilling the secondary frequency/voltage restorations.

In order to emphasize the finite-time feature of the proposed controller, it is compared with the existing asymptotic event-triggered controller presented in [26]. The impact of parameter p in (8) on the finite-time consensus characteristic, is also discussed. Figure 6 shows the frequency response of DG 4 to the existing asymptotic event-triggered controller in [26] and the proposed FETC controller. DG 4 is arbitrarily selected among four DGs. When the secondary control is activated at t=2 s, the proposed FETC controller restores the frequency to 60 Hz with more drastic convergence rate than the asymptotic one. It is also observed that the frequency is restored faster when p=0.3 than p=0.5. As shown, the finite-time strategy can provide faster restoration rate along with the event-triggered controller, with smaller p providing the faster convergence rate.

The impacts followed by different values of φ_0 and ψ on the event-triggered control characteristic are discussed in this paragraph. The frequency response and event occurrence of DG 4 with different φ_0 are given in Fig. 7. φ_0 determines the initial value of a threshold. It can be intuitively thought that the smaller the threshold is, the more communication is triggered. Figure 7a shows the FETC threshold and eventtriggered time for $\varphi_0 = 5$, $\varphi_0 = 10$, and $\varphi_0 = 15$. As expected, communication is triggered the least and the most when $\varphi_0 = 5$ and $\varphi_0 = 15$, respectively. It is shown in Fig. 7b that lesser communications followed by a larger φ_0 lead to a higher oscillation in frequency response. The parameter ψ has impact in the curvature of the threshold as shown in Fig. 8a. Note that ψ affects the initial value of the threshold, but in order to observe sole impact of ψ , χ has been adjusted to make the initial threshold values the same for all cases. As seen, the communication is triggered the least when $\psi = 0.1$, and it can be said that smaller ψ decreases chances of triggering as it expands the area where the error term is smaller than the threshold. In Fig. 8b, it is presented that sparse communication accompanied by a smaller ψ leads to a higher oscillation until it reaches consensus.

2) Case A.2. FETC Under Load Changes: An additional amount of P = 4 kW is applied to and removed from Load 1 at t = 11 s and t = 15 s, respectively. Figure 9 shows the frequencies and active power ratios of DGs. Before the load addition, the system is stably maintained at 60 Hz while properly distributing the active powers among DGs. When load is added at t = 11 s, the system experiences deviations in frequencies and active power ratios. The proposed controller successfully restores the frequencies to 60 Hz and stabilizes the active power sharing approximately within 3 s as can be seen in Fig. 9a and Fig. 9b, respectively. Likewise, when the additional load is removed at t = 15 s, the system confronts the deviation from the nominal states but shortly restored to its desired states by the secondary controller. Figure 10 shows the critical bus voltage and reactive power ratios of DGs. As shown in Fig. 10a, the proposed controller can effectively restore the critical bus voltage to 480 V from the deviation caused by the load changes. After t = 18 s, DGs' Reactive powers are shared proportionally based on DGs' reactive

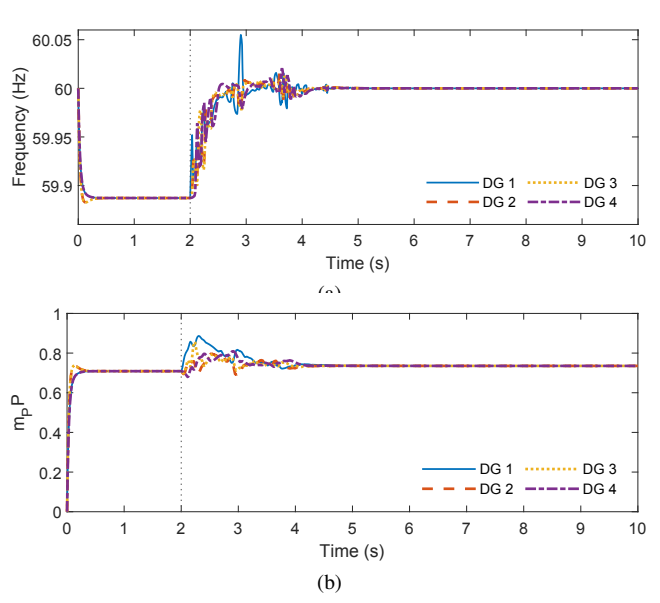


Fig. 4. The FETC frequency control and active power sharing during MG islanding event in *Case A.1*: (a) DG frequencies; (b) active power ratios $m_{Pi}P_i$.

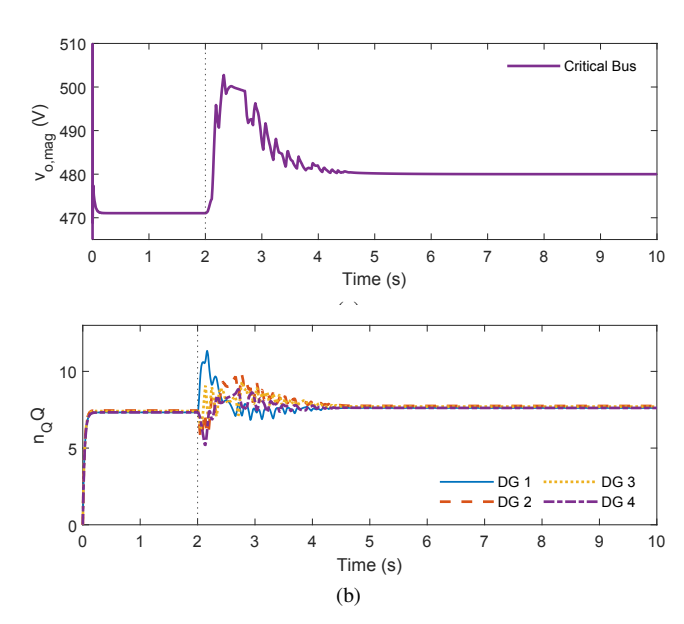


Fig. 5. The FETC voltage control and reactive power sharing during MG islanding event in *Case A.1*: (a) critical bus voltage; (b) reactive power ratios $n_{Qi}Q_i$.

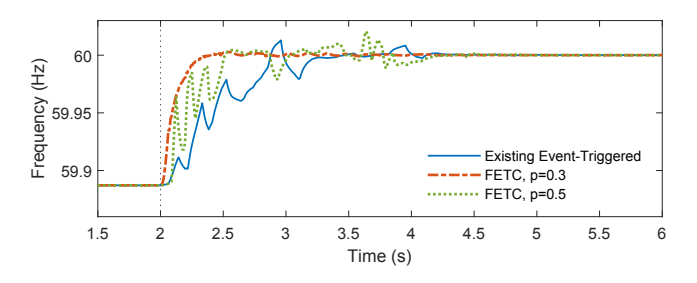


Fig. 6. Frequency response of DG 4 to the existing event-triggered controller in [26] and FETC controller in *Case A.1*.

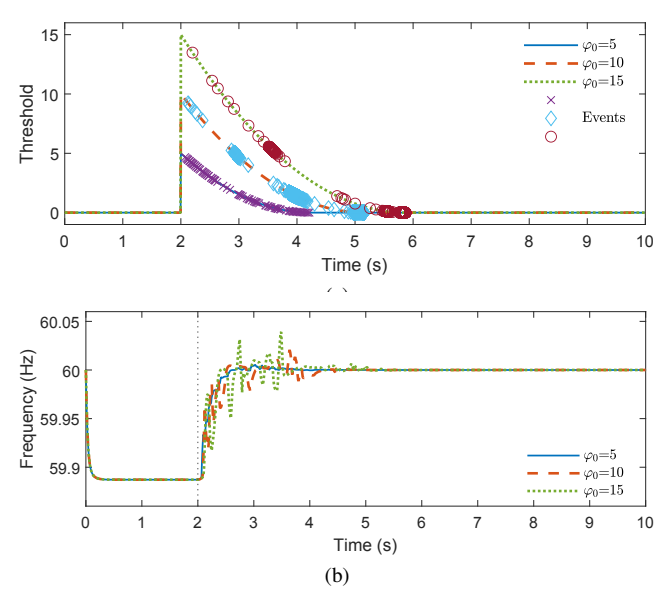


Fig. 7. The impact of φ_0 on the event-triggered control characteristic in *Case A.1*: (a) event-triggering threshold and communication event instances; (b) frequency of DG 4.

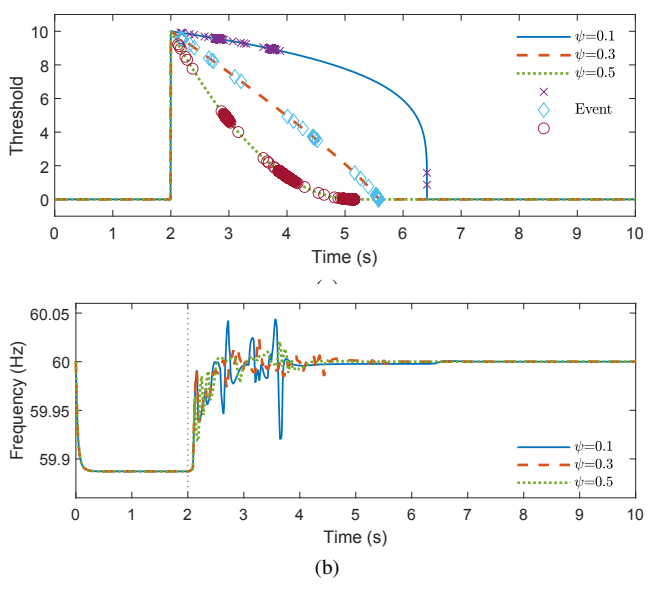


Fig. 8. The impact of ψ on the event-triggered control characteristic in *Case A.1*: (a) event-triggering threshold and communication event instances; (b) frequency of DG 4.

power ratings as shown in Fig. 10b.

3) Case A.3. Plug-and-Play: DG 3 is disconnected from and reconnected to the MG at t=11 s and t=15 s, respectively. Its disconnection and re-connection is projected on the network graph as well. The frequencies and the active power ratios of DGs are given in Fig. 11. Once DG 3 is disconnected at t=11 s, its frequency and active power ratio no longer synchronize with the rest of DGs. On the other hand, DG 1, DG 2, and DG 4 are maintained at the consensus state by the proposed secondary controller even after the disconnection as the graph is still tied to the leader node through DG 1, and is strongly connected. After DG 3 is reconnected at t=15 s, its frequency and active power ratio are synchronized back to the rest of DGs and the system

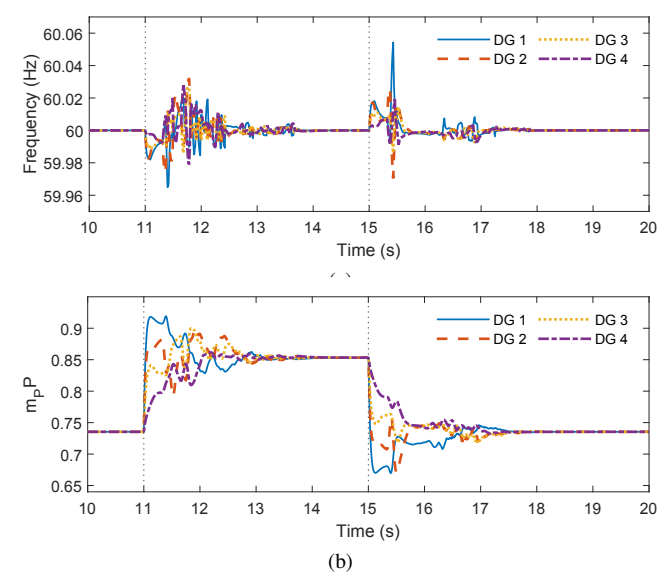


Fig. 9. The FETC frequency control and active power sharing under load changes in *Case A.2*: (a) DG frequencies; (b) active power ratios $m_{Pi}P_i$.

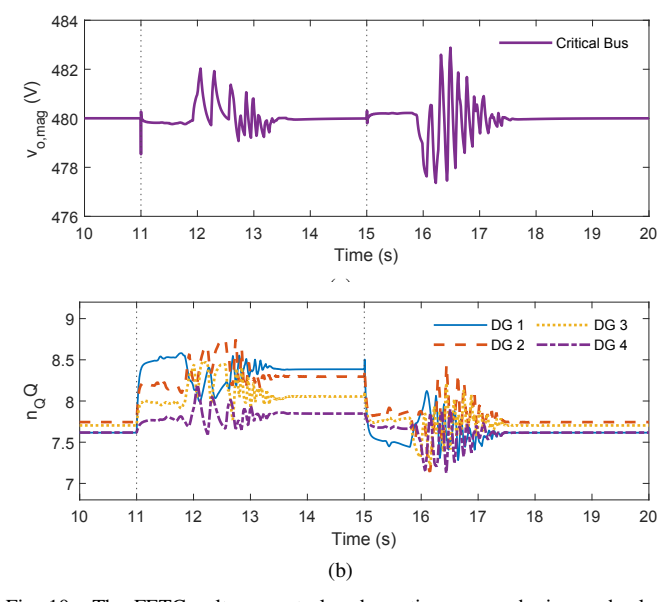


Fig. 10. The FETC voltage control and reactive power sharing under load changes in $Case\ A.2$: (a) critical bus voltage; (b) reactive power ratios $n_{Qi}Q_i$.

reaches consensus at 60 Hz by the secondary controller. The critical bus voltage control and reactive power sharing are also fulfilled by the secondary controller as shown in Fig. 12.

4) Case A.4. Resilience against Communication Link Failures: A continuous and repeated communication graph changes are assumed as depicted in Fig. 13. Graphs in Fig. 13 represent a situation where one or more of the communication links have failed. Each graph is maintained for 0.05 s and repeated throughout the simulation. The event of DG islanding in Case A.1 is simulated under the network graph changes, and the results are given in Fig. 14 and Fig. 15. As shown in the figures, the proposed secondary controllers are capable of fulfilling the frequency/voltage restorations as well as obtaining the active/reactive power sharing.

5) Case A.5. Operation Under Communication Delays: In this test case, the performance of the proposed controller

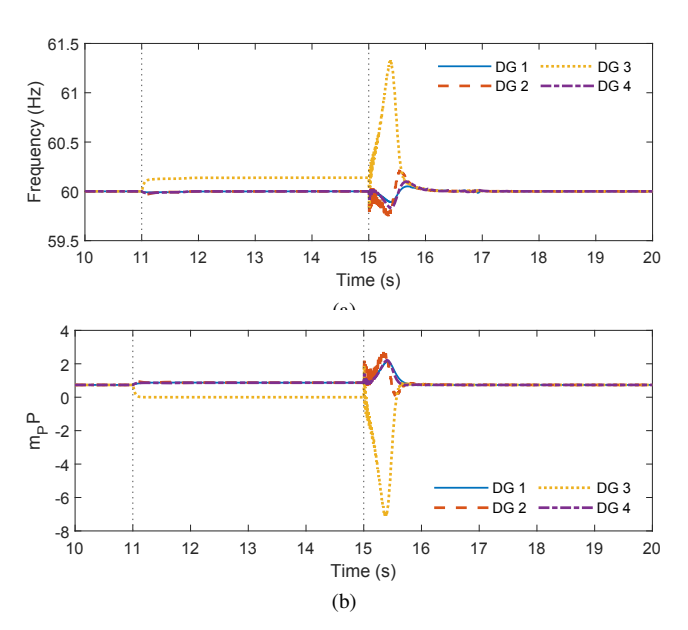


Fig. 11. The FETC frequency control and active power sharing during DG 3 connection and disconnection in *Case A.3*: (a) DG frequencies; (b) active power ratios $m_{Pi}P_i$.

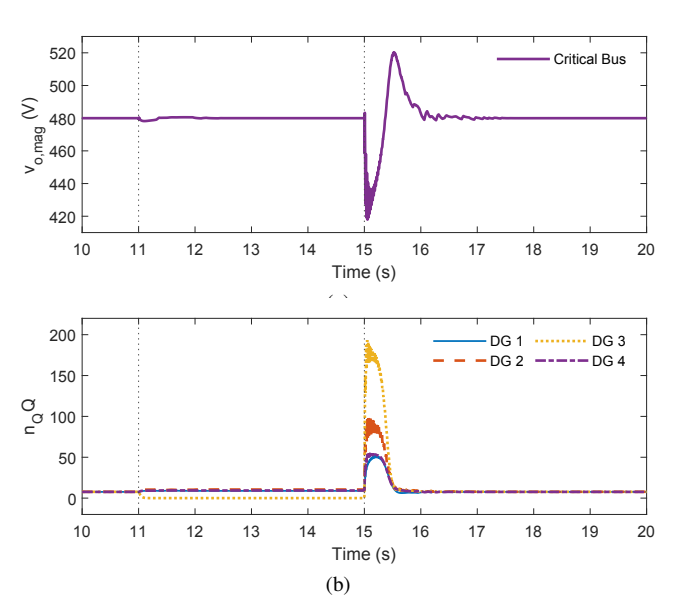


Fig. 12. The FETC voltage control and reactive power sharing during DG 3 connection and disconnection in *Case A.3*: (a) critical bus voltage; (b) reactive power ratios $n_{Qi}Q_i$.

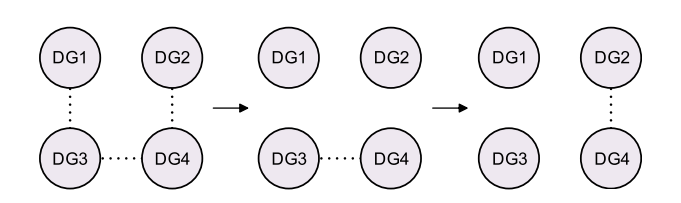


Fig. 13. Graph changes every 0.05s.

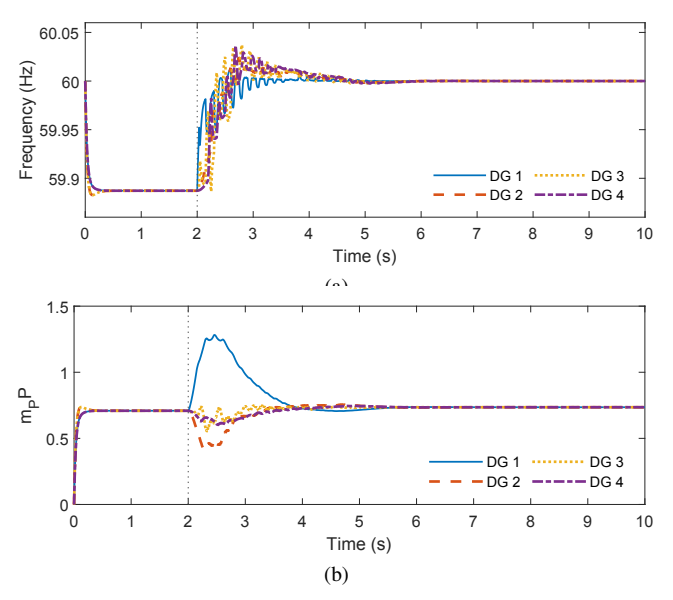


Fig. 14. The FETC frequency control and active power sharing under communication link failures in *Case A.4*: (a) DG frequencies; (b) active power ratios $m_{Pi}P_i$.

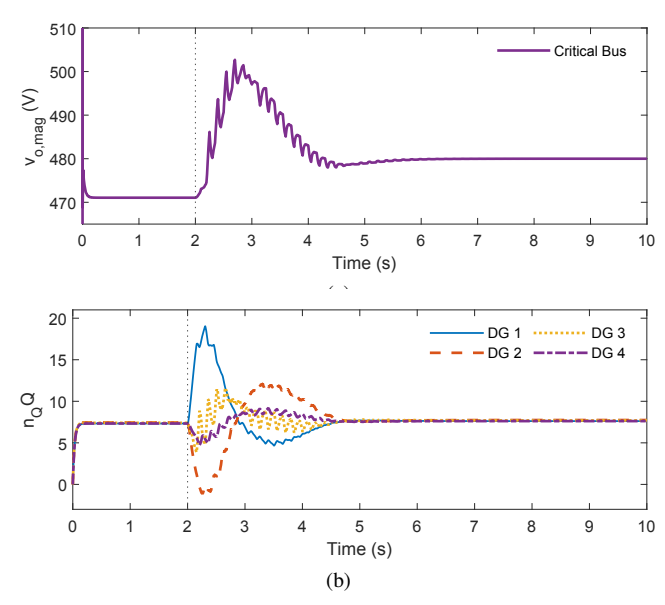


Fig. 15. The FETC voltage control and reactive power sharing under communication link failures in *Case A.4*: (a) critical bus voltage; (b) reactive power ratios $n_{Qi}Q_i$.

under the presence of communication delays is evaluated. The system responses at the event of islanding under the delay of 10 ms and 100 ms are given in Fig. 16 and Fig. 17. Such delays are selected as the communication delays are known to be in range of milliseconds to tens of milliseconds [39], [40]. As shown in the figures, the increase in delays result in larger oscillations in system response, leading to a slower convergence rate. However, the proposed controller is still capable of fulfilling the secondary frequency/voltage and active/reactive power sharing goals.

B. Case B: HIL Verification for Islanded MG with 4 DGs

The 4 DG MG test system model in Fig. 3 that is verified in Case A, is tested in the HIL platform in Case B. The

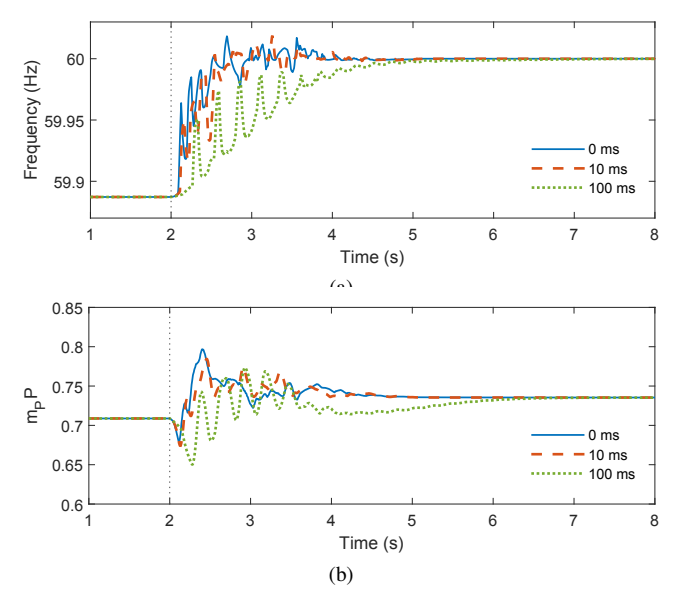


Fig. 16. The FETC frequency control and active power sharing under communication delays plotted for DG 4 in *Case A.5*: (a) frequency of DG 4; (b) active power ratio $m_{Pi}P_i$ of DG 4.

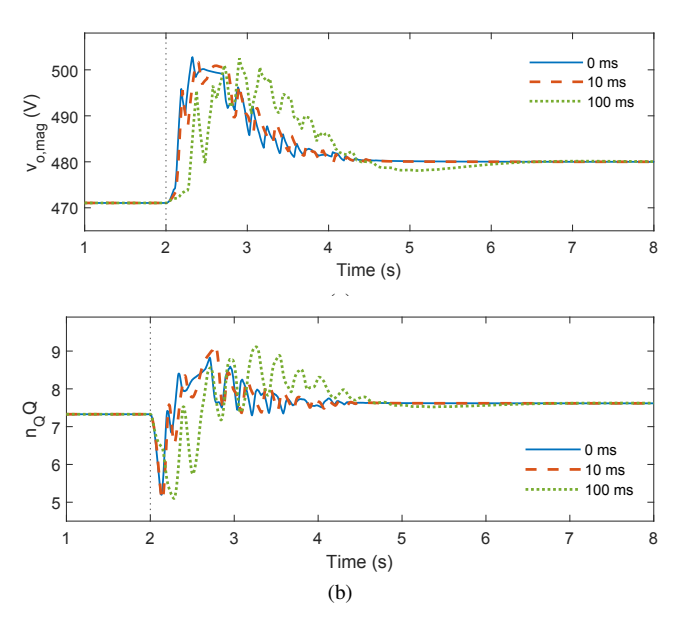


Fig. 17. The FETC voltage control and reactive power sharing under communication delays plotted for DG 4 in Case A.5: (a) critical bus voltage; (b) reactive power ratio $n_{Qi}Q_i$ of DG 4.

control parameters selected for this test case is tabulated in Table III. The HIL platform is implemented as illustrated in Fig. 18. Opal-RT is used for a real-time simulator, and MG test system model in Fig. 3 is simulated in Opal-RT with the time step size of 100 μ s. The proposed secondary controller of each DG is implemented in an individual Raspberry Pi, accommodated in a script written in Python. As shown in Fig. 18, there are two communications required in the implemented HIL platform: communication between OPAL-RT (MG model) and Raspberry Pis shown in orange dashed lines, and between Raspberry Pis in blue dotted lines. Note that the latter represents the network graph among DGs. Both communications required are realized by Ethernet;

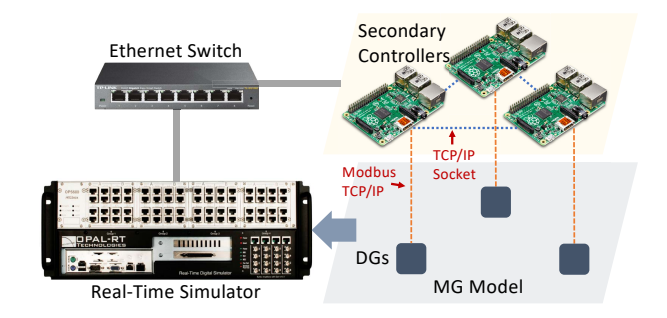


Fig. 18. HIL testbed with Opal-RT and Raspberry Pis.

TABLE III CONTROLLER PARAMETERS IN CASE B

secondary	c_1	c_2	p	secoi	ndary	c_1	c_2	p
Frequency	6	1	0.5	Voltage Reactive Power		10	1	0.5
Active Power	6	1	0.5			10	1	0.5
Triggering Condition	α	β	γ	χ	$arepsilon_1$	$arepsilon_2$	ψ	$arphi_0$
$f_{Pi} \ f_{Qi}$	17 31	76 202	13 33	1 1	1 1	1.1 1.1	0.5 0.5	30 50

OPAL-RT and the Raspberry Pis are connected to Ethernet switches under the same network. The data between each DG and its corresponding controller is transferred via Modbus TCP/IP. Each DG in the model and each controller serves as Modbus slave and master, respectively. The communication graph across controllers is realized on TCP/IP socket. The HIL simulation is processed in the following sequence; with an average measurement sampling and controller updating cycle of 6.77 ms.

- The measurements from DG i, \(\omega_i\), \(P_i\), \(v^*_{o,\text{mag}i}\), and \(Q_i\), are sent to the corresponding controller via Modbus TCP/IP.
- 2) If the event-triggering condition is satisfied, the controller i transmits ω_i , P_i , $v_{o,\mathrm{mag}i}^*$, and Q_i to its outneighbor controllers via TCP/IP socket, i.e., controllers j that are $a_{ji} > 0$; and controller i receives ω_j , P_j , $v_{o,\mathrm{mag}j}^*$, and Q_j from its in-neighbors, i.e., controllers j that are $a_{ij} > 0$.
- 3) The controller i then calculates ω_{ni} and v_{ni} using (16) and (2), and sends ω_{ni} and v_{ni} to DG i in the model through Modbus TCP/IP.
- 1) Case B.1. Islanding from Main Grid: The performance of the proposed controller when MG is islanded, is evaluated in this test case. The results are given in Fig. 19 and Fig. 20. Initially, MG is in an islanded mode and the system is stabilized without the secondary control applied during $0 \le t \le 5$ s. As shown in Fig. 19a, the frequency is settled at 59.9 Hz, deviated from the nominal frequency of 60 Hz. The secondary frequency control is activated at t=5 s, and the frequency is restored to 60 Hz around t=25 s. Also, Fig. 19b shows that the active power ratios of all DGs are synchronized to each other before and after the secondary control is applied, implying that the active power sharing is achieved through the

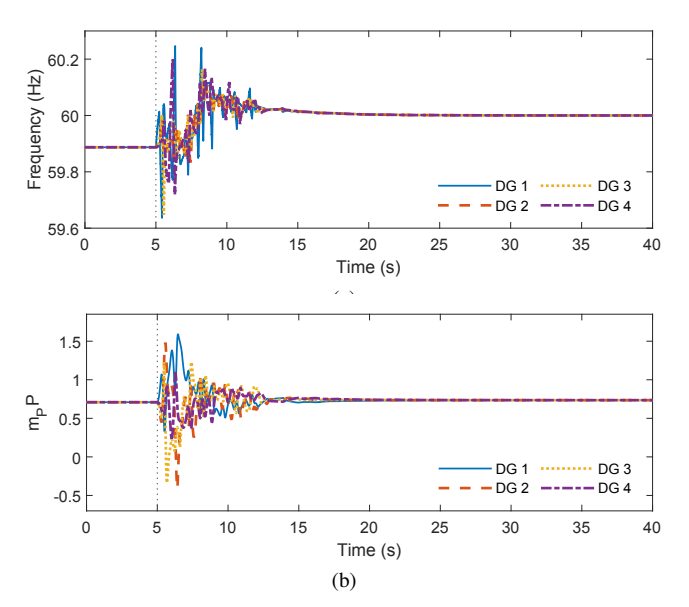


Fig. 19. The FETC frequency control and active power sharing during MG islanding event in *Case B.1*: (a) DG frequencies; (b) active power ratios $m_{Pi}P_i$.

primary control. For the voltage control, $k_p=1$ and $k_i=0.3$ are used to calculate $v_{\rm ref}$. As shown in Fig. 20a, the critical bus voltage is settled around 471 V deviated from 480 V, when the secondary control is not activated. When the secondary voltage controller is applied at t=5 s, the critical bus voltage is restored to 480 V around t=25 s. Figure 20b shows that the proposed controller can also provide the reactive power sharing.

The average event intervals for the frequency/active power and voltage/reactive power sharing control during the transient period $5 \le t \le 25$, are 12.3 ms and 10.6 ms, respectively, whereas it would be 7 ms without the FETC strategy. Therefore it is verified from the HIL test, that the FETC strategy can provide frequency/voltage restoration and active/reactive power sharings in finite-time convergence rate, while reducing the burden in communication network.

2) Case B.2. FETC Under Load Changes: An additional load $P=4~\mathrm{kW}$ is applied to and removed from DG 1 bus at $t=80~\mathrm{s}$ and $t=120~\mathrm{s}$, respectively. The frequencies and the active power ratios of DGs are given in Fig. 21. When the load is added or removed, the frequency deviates from 60 Hz and the synchronization of active power ratios is interrupted. However, the frequency is restored to 60 Hz around $t=95~\mathrm{Hz}$ and the active power ratios are synchronized again. The critical bus voltage and the reactive power ratios are shown in Fig. 22. Likewise, the critical bus voltage is restored to 480 V from deviation caused by the load changes, while providing a proper reactive power sharing.

C. Case C: Model Verification for Islanded MG with 20 DGs

In order to test the scalability of the proposed controller, it is applied to a 20 DG MG test system illustrated in Fig. 23a. The specifications of the MG model are listed in Table IV. The communication network for this test case, is designed as illustrated in Fig. 23b. DG 1 has a direct edge from the

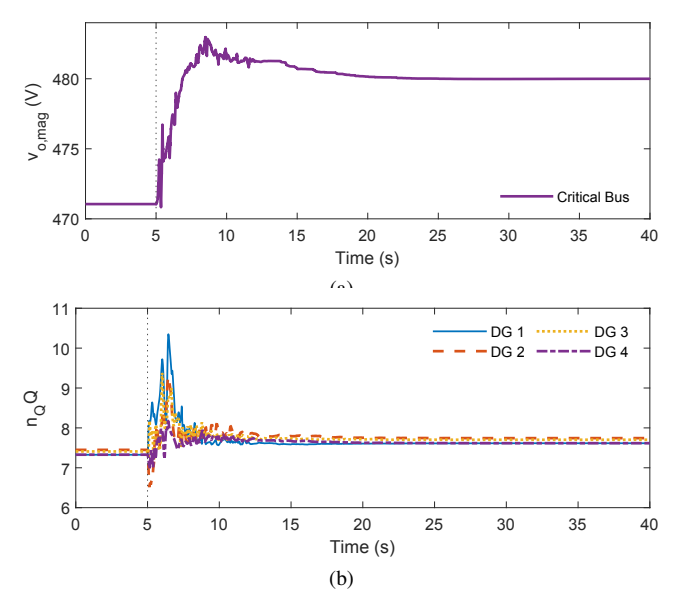


Fig. 20. The FETC voltage control and reactive power sharing during MG islanding event in *Case B.1*: (a) critical bus voltage; (b) reactive power ratios $n_{Qi}Q_i$.

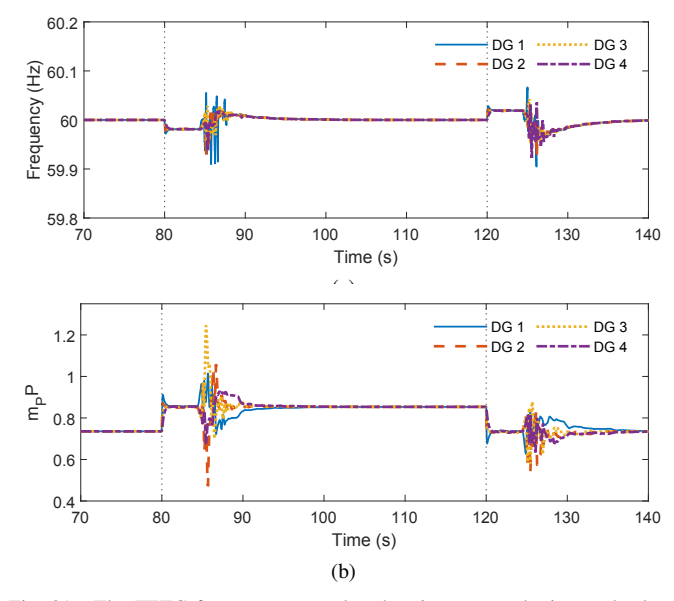


Fig. 21. The FETC frequency control and active power sharing under load changes in *Case B.2*: (a) DG frequencies; (b) active power ratios $m_{Pi}P_i$.

leader node with the pinning gain of $g_1 = 1$. The algebraic connectivity of the given graph is $a(\mathcal{L}) = 5.6180$. The FETC controller and the event-triggering function are configured by the parameters provided in Table V. The output frequencies and the active power ratios of the DGs under the given control configuration, are shown in Fig. 24. In Fig. 24a after the disconnection from the main grid at t = 0, the frequencies start to diverge from the nominal frequency of 60 Hz. The secondary control acts at t = 1 s and the frequency is restored to 60 Hz at t = 5 s, while providing the successful active power sharing as shown in Fig. 24b. The communication triggering timestamps for each DG are shown in Fig. 25. The average communication interval of the proposed FETC-based control during 1 < t < 5 s, is 0.19 ms.

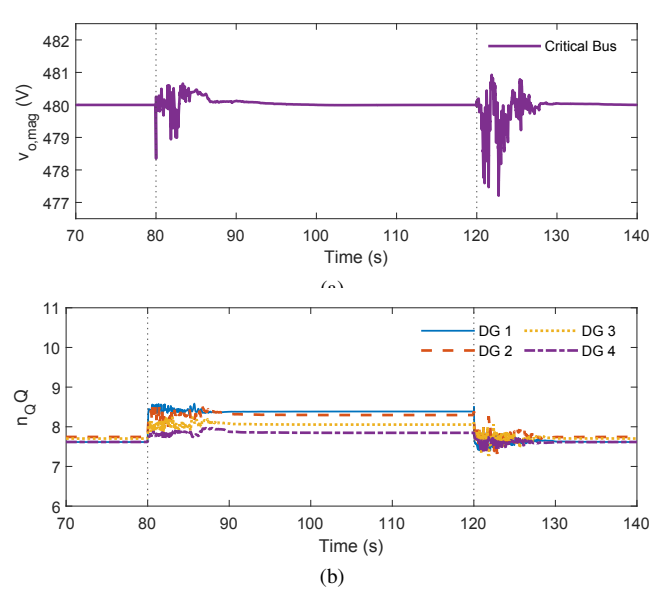
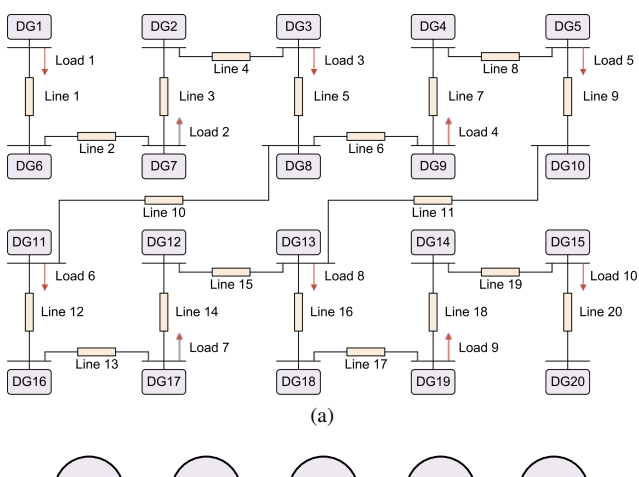


Fig. 22. The FETC voltage control and reactive power sharing under load changes in $Case\ B.2$: (a) critical bus voltage; (b) reactive power ratios $n_{Qi}Q_i$.

$\begin{array}{c} \text{TABLE IV} \\ \text{MG Specifications in Case C} \end{array}$

DGs	DG 1 - 5, 11 - 15	DG 6 - 10, 16 - 20
m_P	4×10^{-5}	6×10^{-5}
n_Q	1.3×10^{-3}	1.5×10^{-3}
$R_{\rm c}$	$0.03~\Omega$	$0.03~\Omega$
$L_{\rm c}$	0.35 mH	0.35 mH
$R_{ m f}$	$0.1~\Omega$	$0.1~\Omega$
$L_{ m f}$	1.35 mH	1.35 mH
$C_{ m f}$	$50~\mu\mathrm{F}$	$50~\mu\mathrm{F}$
$K_{ m PV}$	0.1	0.05
K_{IV}	420	390
K_{PC}	15	10.5
$K_{\rm IC}$	20000	16000
Lines	Line 1, 3, 4, 6, 7, 9, 10, 12, 13, 15, 16, 18, 19	Line 2, 5, 8, 11, 14, 17, 20
R	$0.23~\Omega$	$0.35~\Omega$
X	$0.1~\Omega$	$0.58~\Omega$
Loads	Load 1, 3, 5, 7, 9	Load 2, 4, 6, 8, 10
\overline{P}	30 kW	45.9 kW
Q_L	$10~\mathrm{kVAr}$	$22~\mathrm{kVAr}$
Q_C	0 kVAr	0 kVAr



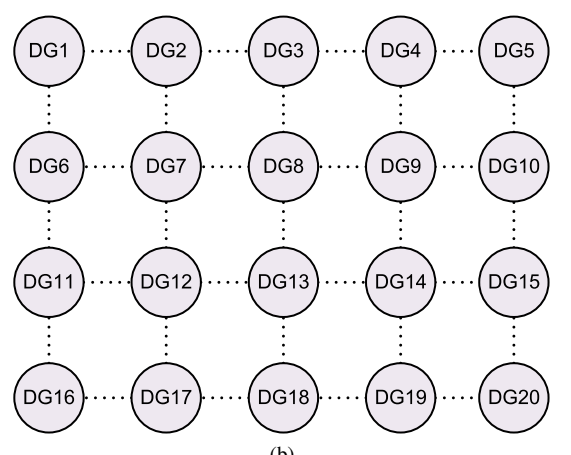


Fig. 23. 20 DG MG test system in $Case\ C$: (a) circuit diagram; (b) communication graph.

TABLE V CONTROLLER PARAMETERS IN CASE C

secondary	c_1	c_2	p	Active Power		c_1	c_2	p
Frequency	50	10	0.5			50	10	0.5
Triggering Condition	α	β	γ	χ	$arepsilon_1$	$arepsilon_2$	ψ	φ_0
f_{Pi}	34	552	60	1	1	5	0.5	50

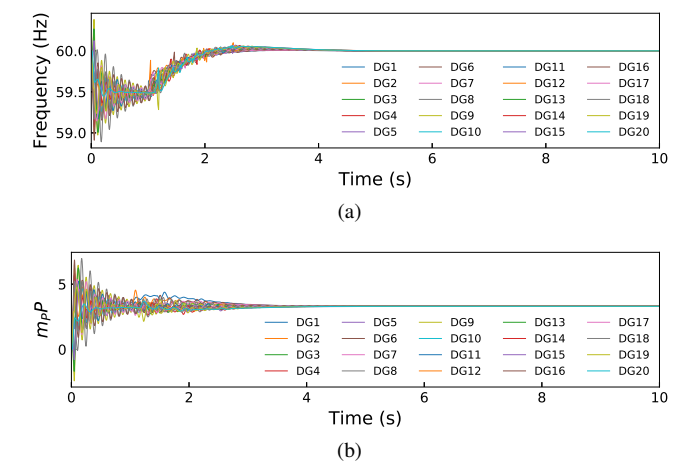


Fig. 24. The FETC frequency control and active power sharing in *Case C*: (a) DG frequencies; (b) active power ratios $m_{Pi}P_i$.

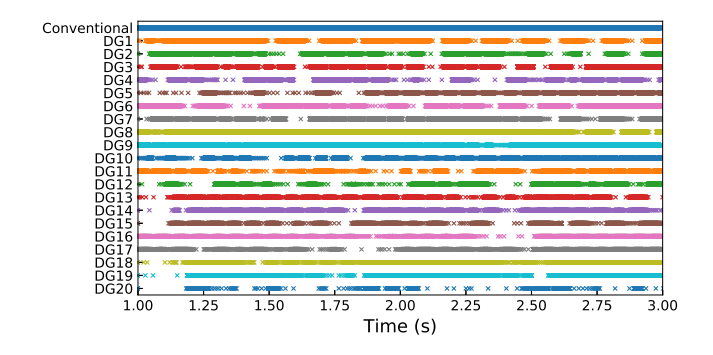


Fig. 25. Communication triggered time of DGs in Case C.

V. CONCLUSION

This paper proposes a FETC control strategy for the secondary frequency and voltage regulation of the distributed MGs. The proposed strategy controls MG frequency and voltage while sharing the active and reactive power among the DGs based on their ratings. The proposed FETC control provides the system consensus in finite-time as well as reducing the communication energy compared to the continuous communication controller. The model simulation results using 4 DG MG test system, suggest the efficacy of the proposed controller, supporting with various test cases: response at an islanding event, load changes, plug-and-play, communication link failures, and communication delays. The HIL simulation results further strengthen the effectiveness of the proposed strategy with two case studies: islanding event and load changes. The scalability of the proposed controller is also verified through the simulation in a 20 DG test MG system. The future research directions will include investigating the cyber security of FETC secondary control of microgrids and creating attack resilient FETC control techniques.

REFERENCES

- J. M. Guerrero, J. C. Vasquez, J. Matas, L. G. De Vicuña, and M. Castilla, "Hierarchical control of droop-controlled ac and dc microgrids—a general approach toward standardization," *IEEE Trans. Ind. Electron.*, vol. 58, no. 1, pp. 158–172, Jan. 2011.
- [2] A. Bidram and A. Davoudi, "Hierarchical structure of microgrids control system," *IEEE Trans. Smart Grid*, vol. 3, no. 4, pp. 1963–1976, Dec. 2012.
- [3] A. Bidram, A. Davoudi, F. L. Lewis, and J. M. Guerrero, "Distributed cooperative secondary control of microgrids using feedback linearization," *IEEE Trans. Power Syst.*, vol. 28, no. 3, pp. 3462–3470, Aug. 2013.
- [4] A. Bidram, A. Davoudi, and F. L. Lewis, "A multiobjective distributed control framework for islanded ac microgrids," *IEEE Trans. Ind. Infor*mat., vol. 10, no. 3, pp. 1785–1798, Aug. 2014.
- [5] Q. Shafiee, J. M. Guerrero, and J. C. Vasquez, "Distributed secondary control for islanded microgrids—a novel approach," *IEEE Trans. Power Electron.*, vol. 29, no. 2, pp. 1018–1031, Feb. 2014.
- [6] J. W. Simpson-Porco, F. Dörfler, and F. Bullo, "Synchronization and power sharing for droop-controlled inverters in islanded microgrids," *Automatica*, vol. 49, no. 9, pp. 2603–2611, Sep. 2013.
- [7] R. Heydari, M. S. Golsorkhi, M. Savaghebi, T. Dragicevic, and F. Blaabjerg, "Communication-free secondary frequency and voltage control of vsc-based microgrids: A high-bandwidth approach," in 22nd European Conference on Power Electronics and Applications (EPE'20 ECCE Europe), 2020, pp. 1–9.
- [8] S. Li, H. Du, and X. Lin, "Finite-time consensus algorithm for multiagent systems with double-integrator dynamics," *Automatica*, vol. 47, no. 8, pp. 1706–1712, Aug. 2011.

- [9] X. Lu, R. Lu, S. Chen, and J. Lu, "Finite-time distributed tracking control for multi-agent systems with a virtual leader," *IEEE Trans. Circuits Syst. I, Reg. Papers*, vol. 60, no. 2, pp. 352–362, Feb. 2013.
- [10] Z.-H. Guan, F.-L. Sun, Y.-W. Wang, and T. Li, "Finite-time consensus for leader-following second-order multi-agent networks," *IEEE Trans. Circuits Syst. I, Reg. Papers*, vol. 59, no. 11, pp. 2646–2654, Nov. 2012.
- [11] J. Bickel, "An overview of transients in power systems," 2019, [Online]. Available: https://download.schneider-electric.com/files?p_enDocType= White+Paper&p_File_Name=998-20579579_GMA.pdf&p_Doc_Ref= 998-20579579_GMA.
- [12] A. Bidram, A. Davoudi, and F. Lewis, "Finite-time frequency synchronization in microgrids," in *IEEE Energy Conversion Congress and Exposition (ECCE)*, 2014, pp. 2648–2654.
- [13] F. Guo, C. Wen, J. Mao, and Y.-D. Song, "Distributed secondary voltage and frequency restoration control of droop-controlled inverter-based microgrids," *IEEE Trans. Ind. Electron.*, vol. 62, no. 7, pp. 4355–4364, July 2015.
- [14] S. Zuo, A. Davoudi, Y. Song, and F. L. Lewis, "Distributed finite-time voltage and frequency restoration in islanded ac microgrids," *IEEE Trans. Ind. Electron.*, vol. 63, no. 10, pp. 5988–5997, Oct. 2016.
- [15] N. M. Dehkordi, N. Sadati, and M. Hamzeh, "Distributed robust finite-time secondary voltage and frequency control of islanded microgrids," *IEEE Trans. Power Syst.*, vol. 32, no. 5, pp. 3648–3659, Sept. 2017.
- [16] D. V. Dimarogonas, E. Frazzoli, and K. H. Johansson, "Distributed event-triggered control for multi-agent systems," *IEEE Trans. Autom. Control*, vol. 57, no. 5, pp. 1291–1297, May 2012.
- [17] E. Garcia, Y. Cao, and D. W. Casbeer, "Decentralized event-triggered consensus with general linear dynamics," *Automatica*, vol. 50, no. 10, pp. 2633–2640, Oct. 2014.
- [18] C. Nowzari and J. Cortés, "Zeno-free, distributed event-triggered communication and control for multi-agent average consensus," in 2014 American Control Conference. IEEE, 2014, pp. 2148–2153.
- [19] Y. Fan, G. Hu, and M. Egerstedt, "Distributed reactive power sharing control for microgrids with event-triggered communication," *IEEE Trans. Control Syst. Technol.*, vol. 25, no. 1, pp. 118–128, Jan. 2017.
- [20] M. Chen, X. Xiao, and J. M. Guerrero, "Secondary restoration control of islanded microgrids with a decentralized event-triggered strategy," *IEEE Trans. Ind. Informat.*, vol. 14, no. 9, pp. 3870–3880, Sept. 2018.
- [21] L. Ding, Q.-L. Han, and X.-M. Zhang, "Distributed secondary control for active power sharing and frequency regulation in islanded microgrids using an event-triggered communication mechanism," *IEEE Trans. Ind. Informat.*, vol. 15, no. 7, pp. 3910–3922, July 2019.
- [22] S. Weng, D. Yue, C. Dou, J. Shi, and C. Huang, "Distributed event-triggered cooperative control for frequency and voltage stability and power sharing in isolated inverter-based microgrid," *IEEE Trans. Cybern.*, vol. 49, no. 4, pp. 1427–1439, Apr. 2019.
- [23] T. Qian, Y. Liu, W. Zhang, W. Tang et al., "Event-triggered updating method in centralized and distributed secondary controls for islanded microgrid restoration," *IEEE Trans. Smart Grid*, vol. 11, no. 2, pp. 1387– 1395, Mar. 2020.
- [24] B. Abdolmaleki, Q. Shafiee, M. M. Arefi, and T. Dragičević, "An instantaneous event-triggered hz-watt control for microgrids," *IEEE Trans. Power Syst.*, vol. 34, no. 5, pp. 3616–3625, Sept. 2019.
- [25] B. Abdolmaleki, Q. Shafiee, A. R. Seifi, M. M. Arefi, and F. Blaabjerg, "A zeno-free event-triggered secondary control for ac microgrids," *IEEE Trans. Smart Grid*, vol. 11, no. 3, pp. 1905–1916, May 2020.
- [26] Y. Wang, T. L. Nguyen, Y. Xu, Z. Li, Q.-T. Tran, and R. Caire, "Cyber-physical design and implementation of distributed event-triggered secondary control in islanded microgrids," *IEEE Trans. Ind. Appl.*, vol. 55, no. 6, pp. 5631–5642, Nov. 2019.
- [27] Y. Zhu, X. Guan, X. Luo, and S. Li, "Finite-time consensus of multi-agent system via nonlinear event-triggered control strategy," *IET Control Theory Appl.*, vol. 9, no. 17, pp. 2548–2552, Nov. 2015.
- [28] H. Zhang, D. Yue, X. Yin, S. Hu, and C. xia Dou, "Finite-time distributed event-triggered consensus control for multi-agent systems," *Inf. Sci.*, vol. 339, pp. 132–142, Apr. 2016.
- [29] Q. Lu, Q.-L. Han, B. Zhang, D. Liu, and S. Liu, "Cooperative control of mobile sensor networks for environmental monitoring: An eventtriggered finite-time control scheme," *IEEE Trans. Cybern.*, vol. 47, no. 12, pp. 4134–4147, Dec. 2017.
- [30] Y. Dong and J.-g. Xian, "Finite-time event-triggered consensus for non-linear multi-agent networks under directed network topology," *IET Control Theory Appl.*, vol. 11, no. 15, pp. 2458–2464, Oct. 2017.
- [31] Z. Cao, C. Li, X. Wang, and T. Huang, "Finite-time consensus of linear multi-agent system via distributed event-triggered strategy," *J. Franklin Inst.*, vol. 355, no. 3, pp. 1338–1350, Feb. 2018.

- [32] J. Li, X. Wu, Q. Li, and Y. Li, "Finite-time distributed event-triggered consensus control for leader-following general linear multi-agent systems," in *IEEE 3rd Advanced Information Technology, Electronic and Automation Control Conference (IAEAC)*, 2018, pp. 1974–1978.
- [33] L. Zhang, Z. Zhang, N. Lawrance, J. Nieto, and R. Siegwart, "Decentralised finite-time consensus for second-order multi-agent system under event-triggered strategy," *IET Control Theory Appl.*, vol. 14, no. 4, pp. 664–673, Mar. 2020.
- [34] C. Du, X. Liu, W. Ren, P. Lu, and H. Liu, "Finite-time consensus for linear multi-agent systems via event-triggered strategy without continuous communication," *IEEE Trans. Control Netw. Syst.*, vol. 7, no. 1, pp. 19–29, Mar. 2020.
- [35] A. Bidram, F. L. Lewis, and A. Davoudi, "Synchronization of non-linear heterogeneous cooperative systems using input-output feedback linearization," *Automatica*, vol. 50, no. 10, pp. 2578–2585, 2014.
- [36] A. Bidram, V. Nasirian, A. Davoudi, and F. L. Lewis, Cooperative synchronization in distributed microgrid control. Springer, 2017.
- [37] W. Yu, G. Chen, M. Cao, and J. Kurths, "Second-order consensus for multiagent systems with directed topologies and nonlinear dynamics," *IEEE Trans. Syst., Man, Cybern. B, Cybern.*, vol. 40, no. 3, pp. 881–891, June 2010.
- [38] S. P. Bhat and D. S. Bernstein, "Finite-time stability of continuous autonomous systems," SIAM Journal on Control and Optimization, vol. 38, no. 3, pp. 751–766, 2000.
- [39] Q. Shafiee, Č. Stefanović, T. Dragičević, P. Popovski, J. C. Vasquez, and J. M. Guerrero, "Robust networked control scheme for distributed secondary control of islanded microgrids," *IEEE Tran. Ind. Electron.*, vol. 61, no. 10, pp. 5363–5374, Oct. 2014.
- [40] C. Ahumada, R. Cárdenas, D. Saez, and J. M. Guerrero, "Secondary control strategies for frequency restoration in islanded microgrids with consideration of communication delays," *IEEE Trans. Smart Grid*, vol. 7, no. 3, pp. 1430–1441, Aug. 2015.



Ali Bidram (S'12-M'17-SM'20) is currently an Assistant Professor in the Electrical and Computer Engineering Department, University of New Mexico, Albuquerque, NM, USA. He has received his B.Sc. and M.Sc. from Isfahan University of Technology, Iran, in 2008 and 2010, and Ph.D. from the University of Texas at Arlington, USA, in 2014. Before joining University of New Mexico, he worked with Quanta Technology, LLC, and was involved in a wide range of projects in electric power industry. He is an Associate Editor for the IEEE Transactions

on Industry Applications.

His area of expertise lies within control and coordination of energy assets in power electronics-intensive energy distribution grids. Such research efforts are culminated in a book, several journal papers in top publication venues and articles in peer-reviewed conference proceedings, and technical reports. He has received IEEE Albuquerque section outstanding engineering educator award, New Mexico EPSCoR mentorship award, University of Texas at Arlington N. M. Stelmakh outstanding student research award, Quanta Technology Shooting Star award, IEEE Kansas Power and Energy Conference best paper award, and cover article of December 2014 in IEEE Control Systems.



Jeewon Choi (S'20) received the B.S. degree in mechanical and automotive engineering from Keimyung University, Daegu, South Korea, in 2015, and M.S. degree in mechanical engineering from the University of New Mexico, Albuquerque, NM, USA, in 2018, where she is currently pursuing the Ph.D. degree in mechanical engineering. Her research interests include smart grid, microgrid, and cyber-physical system modeling and simulation.



Seyed Iman Habibi (S'21) received his B.Sc. and M.Sc. degrees in electrical engineering from K. N. Toosi University of Technology, Tehran, Iran, in 2015 and 2018. He is currently a Ph.D. student in the University of New Mexico. His main research areas include secondary control of microgrids, supervisory control, switching control, and adaptive systems.